N72-33211

NASA CONTRACTOR REPORT

NASA CR-2124

NASA CR-2124

CASE FILE COPY

A FINITE-DIFFERENCE METHOD FOR PREDICTING SUPERSONIC TURBULENT BOUNDARY-LAYER FLOWS WITH TANGENTIAL SLOT INJECTION

by E. W. Miner and C. H. Lewis

Prepared by
VIRGINIA POLYTECHNIC INSTITUTE AND STATE UNIVERSITY
Blacksburg, Va. 24061
for Langley Research Center

NATIONAL AERONAUTICS AND SPACE ADMINISTRATION • WASHINGTON, D. C. • OCTOBER 1972

1. Report No.	2. Government Accession No.	3. Recipient's Catalog No.
NASA CR-2124		

4. Title and Subtitle	5. Report Date
A FINITE-DIFFERENCE METHOD FOR PREDICTING SUPERSONIC TURBULENT BOUNDARY-LAYER FLOWS WITH TANGENTIAL SLOT INJECTION	October 1972
	6. Performing Organization Code
7. Author(s)	8. Performing Organization Report No.
E. W. Miner and C. H. Lewis	
	10. Work Unit No.
9. Performing Organization Name and Address	
Aerospace Engineering Department Virginia Polytechnic Institute and State University Blacksburg, VA 24061	11. Contract or Grant No. NGR-47-004-072
	13. Type of Report and Period Covered
12. Sponsoring Agency Name and Address	Contractor Report
National Aeronautics and Space Administration Washington, D.C. 20546	14. Sponsoring Agency Code

15. Supplementary Notes

16. Abstract

An implicit finite-difference method has been applied to tangential slot injection into supersonic turbulent boundary-layer flows. In addition, the effects induced by the interaction between the boundary-layer displacement thickness and the external pressure field are considered.

In the present method, three different eddy viscosity models have been used to specify the turbulent momentum exchange. One model depends on the species concentration profile and the species conservation equation has been included in the system of governing partial differential equations.

Results are compared with experimental data at stream Mach numbers of 2.4 and 6.0 and with results of another finite-difference method. Good agreement was generally obtained for the reduction of wall skin friction with slot injection and with experimental Mach number and pitot pressure profiles. Calculations with the effects of pressure interaction included showed these effects to be smaller than effects of changing eddy viscosity models.

17. Key Words (Suggested by Author(s))	18. Distribution Statement
Tangential injection and mixing Compressible turbulent boundary layers Eddy viscosity models	Unclassified - Unlimited

19. Security Classif. (of this report)	20. Security Classif. (of this page)	21. No. of Pages	22. Price*
Unclassified	Unclassified	78	$3.00

*For sale by the National Technical Information Service, Springfield, Virginia 22151

I. ABSTRACT

An implicit finite-difference method has been developed for the solution of the compressible boundary-layer equations. This method is applied to tangential slot injection into supersonic turbulent boundary-layer flows. In addition, the effects induced by the interaction between the boundary-layer displacement thickness and the external pressure field are considered.

In the present method, three different eddy viscosity models have been used to specify the turbulent momentum exchange. One model depends on the species concentration profile and the species conservation equation has been included in the system of governing partial differential equations. For air injected into air, the freestream and injected gases are treated as separate species which have common fluid properties.

Calculations were made with the present method and results were compared with experimental data at stream Mach numbers of 2.4 and 6.0 and with results of another finite-difference method. Good agreement was obtained for the reduction of wall skin friction with slot injection. Comparison with available experimental Mach number and pitot pressure profiles gave reasonable agreement in most cases. Calculations with the effects of pressure interaction included showed these effects to be smaller than effects of changing eddy viscosity models.

Page intentionally left blank

II. TABLE OF CONTENTS

		Page
I.	ABSTRACT	iii
II.	TABLE OF CONTENTS	v
III.	LIST OF FIGURES	vii
IV.	LIST OF SYMBOLS	ix
V.	INTRODUCTION	1
VI.	ANALYSIS	4
	6.1 Governing Equations	4
	6.1.1 Conservation Equations	4
	6.1.2 Coordinate Transformation	7
	6.1.3 Numerical Solution Procedure	9
	6.1.4 Fluid Properties	9
	6.2 Eddy Viscosity Models	10
	6.2.1 Two-Layer Models	10
	a. Van Driest Inner Law	10
	b. Clauser Outer Law	11
	c. Schetz Outer Law	11
	6.2.2 Multi-Layer Model	12
	a. Mixing Length for Fully Developed Turbulent Flow	12
	b. Modified Mixing Length for Tangential Slot Injection	13
	6.3 Pressure Interaction Effects	16
	6.4 Application of Finite-Difference Method	18
VII.	RESULTS AND DISCUSSION	20
	7.1 Cary's Slot Injection Experimental Conditions	20
	7.2 Kenworthy and Schetz Slot Injection Experimental Conditions	23
	7.3 Computing Time Required	27
VIII.	CONCLUSIONS	30
IX.	REFERENCES	32

Page intentionally left blank

III. LIST OF FIGURES

Figure		Page
1	Schematic of Slot Injection Flow Field	35
2	Skin-Friction Distributions for Flat Plate Flow, NASA Cary Conditions	36
3	Skin-Friction Distributions with Slot Injection, NASA Cary Conditions	37
4	Comparison of Predicted Skin-Friction Distributions with Different Eddy Viscosity Models, NASA Cary Conditions, Case V	40
5	Initial Velocity Profiles for Slot Injection Calculations, NASA Cary Case V Conditions	41
6	Predicted Skin-Friction Distributions with and without Pressure Interaction, NASA Cary Case V Conditions, with Beckwith-Bushnell ϵ^+	42
7	Predicted Wall Static Pressure Distributions with Pressure Interaction, NASA Cary Case V Conditions	43
8	Predicted Wall Shear Stress Distributions for Flat Plate Flow, VPI Conditions	44
9	Comparison of Eddy Viscosity Profiles for Flat Plate Flow at Slot Location, VPI Conditions	45
10	Wall Static Pressure Distributions for Low Pressure Injection, VPI Conditions	46
11	Comparison of Wall Shear Stress Distributions, VPI Conditions	47
12	Comparison of Mach Number Profiles, Low Pressure Injection, VPI Conditions	48
13	Comparison of Mach Number Profiles, Matched Pressure Injection, VPI Conditions	50
14	Comparison of Pitot Pressure Profiles, Low Pressure Injection, VPI Conditions	52
15	Comparison of Pitot Pressure Profiles, Matched Pressure Injection, VPI Conditions	54

Figure		Page
16	Comparison of Predicted Wall Shear Stress Distributions with Different Eddy Viscosity Models, VPI Conditions	56
17	Comparison of Mach Number Profiles with Different Eddy Viscosity Models; Station 1, VPI Conditions	57
18	Comparison of Mach Number Profiles with Different Eddy Viscosity Models; Station 2, VPI Conditions	58
19	Comparison of Mach Number Profiles with Different Eddy Viscosity Models; Station 3, VPI Conditions	59
20	Comparison of Mach Number Profiles with Different Eddy Viscosity Models, Station 4, VPI Conditions	60
21	Comparison of Wall Shear Stress Distributions with Laminar and Turbulent Slot Flow and Mixing, VPI Conditions	61
22	Comparison of Mach Number Profiles with Laminar and Turbulent Slot Flow and Mixing; Station 1, VPI Conditions	62
23	Comparison of Mach Number Profiles with Laminar and Turbulent Slot Flow and Mixing; Station 2, VPI Conditions	63
24	Comparison of Mach Number Profiles with Laminar and Turbulent Slot Flow and Mixing; Station 3, VPI Conditions	64
25	Comparison of Mach Number Profiles with Laminar and Turbulent Slot Flow and Mixing; Station 4, VPI Conditions	65
26	Comparison of Mach Number Profiles with Different Initial Species Concentration Profiles at Station 4 for VPI Conditions	66
27	Comparison of Predicted Wall Shear Stress Distributions with and without Pressure Interaction, VPI Conditions, with Beckwith-Bushnell ϵ^+	67
28	Comparison of Experimental and Predicted Wall Static Pressure Distributions, VPI Conditions	68

IV. LIST OF SYMBOLS

a_j, a_m	eddy viscosity constants
C	density-viscosity product ratio, $\rho\mu/(\rho_e\mu_e)$
$C_{air,w}$	concentration of air at wall
C_f	skin-friction coefficient
C_{f_e}	skin-friction coefficient based on edge conditions
C_{f_∞}	skin-friction coefficient based on freestream conditions
C_{f_o}	skin-friction coefficient for flat plate flow
C_i	mass fraction of species i
C_p	specific heat of perfect gas, $m^2/(sec^2 - {}^oK)$
C_{p_f}	frozen specific heat of gas mixture, $m^2/(sec^2 - {}^oK)$, $\sum_i C_i C_{p_i}$
D_{12}	binary diffusion coefficient, m^2/sec
D_t	turbulent diffusion coefficient, m^2/sec
F	tangential velocity ratio, u/u_e
$\tilde{f}$	form factor, Eq. 43
g	stagnation enthalpy ratio, H/H_e
H	stagnation enthalpy, m^2/sec^2
H_k^*	δ_k^*/θ_k
h	static enthalpy, m^2/sec^2
K	eddy viscosity constant, 0.4
k	thermal conductivity, $J/(m - sec - {}^oK)$
k_1	eddy viscosity constant, 0.4
k_2	eddy viscosity constant, 0.0168
L	reference length, m or cm
Le	molecular Lewis number, $C_{p_f}\ \rho\ D_{12}/k$
Le_t	turbulent Lewis number, $C_{p_f}\ \rho\ D_t/k$

ℓ	mixing length, m or cm
ℓ_b	freestream mixing length, m or cm, $\tilde{f}_s(\delta - y_n)$
ℓ_j	slot mixing length, m or cm, $a_j s/2$
$\ell_{u,m}$	mixing region mixing length, m or cm, $a_m W \, Pr_t/Le_t$
M	Mach number
m_i	molecular weight of species i
P	pressure, N/m^2 or atms
Pr	molecular Prandtl number, $C_{p_f} \mu/k$
Pr_t	turbulent Prandtl number, $C_{p_f} \epsilon/\kappa$
Re	Reynolds number
R_o	universal gas constant
s	slot height, m or cm
T	temperature, ^oK
t	slot lip thickness, m or cm
u	tangential velocity component, m/sec
u^+	friction velocity, m/sec, $(\tau_w/\rho)^{1/2}$
V	transformed normal velocity component, Eqs. 23, 27
v	normal velocity component, m/sec
W	width of mixing region, m or cm, $y_f - y_n$
w	weighting factor, Eq. 56
w_i	production term for species i
x	distance along surface, m or cm
y	distance normal to surface, m or cm
y^+	normal coordinate in law of the wall variables, $y\rho u^+/\mu$
y_f	y at $\tilde{Z} = 0.99$
y_m	y at $\tilde{Z} = 0.5$

y_n y at $\tilde{Z} = 0.01$

y_p y at $Z = 0.5$, Eq. 60

Z mass fraction ratio, C_i/C_{i_e}

$\tilde{Z}$ normalized mass fraction ratio, Eq. 46

β pressure gradient parameter, $\frac{2\xi}{u_e} \frac{du_e}{d\xi}$

γ Klebanoff intermittancy factor, Eq. 37

δ boundary-layer thickness, y at $u/u_e = 0.995$, m or cm

δ_o boundary-layer thickness on flat plate

δ_r $\delta_o + t + s$

δ^* boundary-layer displacement thickness, m or cm, $\int_o^\infty \left[1 - \frac{\rho u}{\rho_e u_e}\right] dy$

δ_k^* incompressible boundary-layer displacement thickness, m or cm, $\int_o^\infty (1 - \frac{u}{u_e})\, dy$ where u is the computed tangential velocity component for compressible flow

ϵ eddy viscosity, N-sec/m^2

ϵ^+ ϵ/μ

ϵ_i^+ inner eddy viscosity

ϵ_o^+ outer eddy viscosity

ϵ_{VD} Van Dyke parameter, $(\rho_\infty^* U_\infty^* L^*/\mu_{ref}^*)^{-1/2}$

η Levy-Lees normal coordinate, $\frac{u_e}{(2\xi)^{1/2}} \int \rho\, dy$

θ_k incompressible boundary-layer momentum thickness, m or cm, $\int_o^\infty \frac{u}{u_e} (1 - \frac{u}{u_e})\, dy$ where u is the computed tangential velocity component for compressible flow

κ turbulent thermal conductivity, J/(m - sec - ^oK)

λ mass flow rate ratio from slot, $\rho_j u_j/(\rho_e u_e)$

μ	viscosity, N-sec/m^2
ξ	Levy-Lees streamwise coordinate, $\int \rho_e \mu_e u_e dx$
ρ	density, kg/m^3
τ_w	shear stress at wall, $\mu \left.\frac{du}{dy}\right\|_w$, N/m^2
τ_{w_o}	wall shear stress for flat plate flow, N/m^2

Subscripts and Superscripts

e	condition at outer edge of boundary layer
i	designates property of species i
j	condition at slot exit
s	denotes limits of integration for δ_k^* and θ_k from y_n to δ instead of from 0 to δ
w	condition at wall boundary
o	stagnation condition, flat plate conditions
ξ	differentiation with respect to ξ
∞	freestream condition
$(\ )'$	differentiation with respect to η

V. INTRODUCTION

During recent years considerable progress has been made in obtaining solutions to the boundary-layer equations. The availability of high-speed, large-scale digital computers has made possible the development of methods of solution which rely on a minimum of assumptions and which are useful over a wide range of conditions.

Davis (Refs. 1, 2, 3) and Blottner (Refs. 4, 5, 6) have been very successful in developing implicit finite-difference methods of the Crank-Nicolson (Ref. 7) type for the solution of the compressible laminar boundary-layer equations. Progress in developing methods of solutions for the compressible turbulent boundary-layer equations came later and more slowly. Among the first well known methods for solving problems of compressible turbulent boundary-layer flows were the finite-difference methods of Spalding and Patankar (Ref. 8), Herring and Mellor (Ref. 9), and Cebeci (Refs. 10, 11). These methods were applied principally to boundary-layer flows over flat plates but were applied to some bodies of revolution. An integral method of solution was developed by Elliott, Bartz, and Silver (Ref. 12) for boundary layers in nozzles and was successfully used by Boldman, Newmann, and Schmidt (Ref. 13) in solving for the heat transfer in rocket nozzles. One drawback of the integral method is the amount of empirical data required.

The early methods of obtaining solutions to the compressible turbulent boundary-layer equations were limited in the range of problems to which the methods could be applied. Further progress in developing finite-difference methods of solution was made by Pletcher (Ref. 14) with an explicit method, by Harris (Ref. 15), and by Bushnell and Beckwith (Ref. 16) with implicit methods of the Crank-Nicolson type. A method similar in the solution procedure to the latter two methods was developed by Anderson and Lewis (Ref. 17) and was applied very successfully to a wide range of problems. The problems to which this method was applied included flat plates, blunt bodies, supersonic and hypervelocity nozzles. Results obtained with this method were reported in Refs. 18 and 19 and the corresponding computer program is described in Ref. 20.

As methods for solving the compressible turbulent boundary-layer equations were developed and applied to an increasingly wide range of problems, progress in aerodynamic research demanded the development of increasingly powerful methods

which could be used both for comparison with experimental data and for predictions of data in cases where experimental results were unavailable. For example, of the methods cited above, only one (Ref. 8) was applied in even a rudimentary way to the problem of film cooling or, equivalently, tangential slot injection into supersonic turbulent boundary-layer flows.

As vehicles have been designed for increasingly high speed flight within the atmosphere, problems of cooling the vehicle have become more severe. As a potential cooling technique, film cooling has been studied both experimentally and numerically. In Ref. 8, a solution was obtained for the tangential slot injection problem by using two flow regions. In the first region, the flow from a planar jet mixed with a boundary-layer flow and the problem was treated as a mixing of two planar flows with the wall region of the flow omitted. When the mixing zone spread to the wall, the solution procedure was switched to the standard technique for turbulent boundary-layer flows. With this approach, Spalding and Patankar were able to evaluate the effects of slot injection starting at some distance downstream of the slot, but were unable to predict wall measurable properties in the region near the slot exit.

In Ref. 21 Cary and Hefner reported preliminary results of their experiment on film cooling effectiveness at Mach 6. Included in Ref. 21 were results of calculations made with the method of Bushnell and Beckwith (Ref. 16) using the modified eddy viscosity expression of Bushnell (Ref. 22). In this eddy viscosity expression, the Prandtl mixing length in the region near the slot (approximately 30 slot heights) is adjusted to account to first order for the effects of slot injection. The mixing length ℓ, in the mixing region downstream of the slot lip, is proportional to the width of the mixing region. Thus near the slot lip ℓ in the mixing region is small and increases downstream with the spread of the region of mixing between the slot and freestream flows. With this eddy viscosity expression, the growth of the mixing region is controlled by a prescribed mixing angle. By using the finite-difference method of Ref. 16 and the eddy viscosity model described in Ref. 22, it was possible to obtain reasonable good agreement with experiment near the slot as well as far downstream of the slot.

By adding the species conservation equation to the system of governing equations, Beckwith and Bushnell (Ref. 23) were able to compute the growth of the

mixing region and the mixing angle was no longer needed. In this work it was assumed that the injected gas and the free stream gas had common properties but were identifiable. The eddy viscosity model was also slightly modified. Cary and Hefner (Ref. 24) compared results obtained with the method of Ref. 23 with their experimental data for matched pressure injection and obtained good agreement for both wall skin friction and wall cooling effectiveness.

In the finite-difference methods of Spalding and Patankar (Ref. 8) and Beckwith and Bushnell (Ref. 23) cited above, it was assumed that the static pressures in the slot and in the freestream were matched. Cary and Hefner (Ref. 24) gave experimental data for unmatched pressure conditions but did not compare with results of the finite-difference method of Ref. 23. Kurkov (Ref. 25) developed finite-difference methods for solving the turbulent boundary-layer equations with a normal pressure gradient included. In Ref. 25 these methods were applied to the mixing of coplanar jets, and the results agreed well with experimental data for pressure distributions. Predicted species concentration profiles were shown but were not compared with experimental data. Kurkov did consider non-matched pressure conditions but restricted the application to jet mixing and presented no results for wall skin friction or wall heat transfer. Also, Kurkov assumed the eddy viscosity depends only on the streamwise coordinate.

In the present work, a finite-difference method for predicting compressible, turbulent boundary-layer flows with tangential slot injection is presented. In this method, the effects induced by the interaction between the boundary-layer displacement thickness and the external pressure field are considered. The inclusion of the species conservation equation in the system of governing equations makes possible predictions of the mixing between the slot and the freestream flows. Three eddy viscosity models are used with the present method.

The governing equations for two-dimensional boundary-layer flow of two-component, nonreacting gas mixtures are presented in physical, dimensional variables. The equations are nondimensionalized and transformed to Levy-Lees variables and the solution procedure is discussed. A global iteration procedure is presented for pressure interaction effects. Calculations were made for tangential slot injection with and without pressure interaction effects included, and the results obtained are compared with the results of Beckwith and Bushnell and with the experimental data of Cary at Mach 6 (Ref. 24) and of Kenworthy and Schetz at Mach 2.4 (Ref. 30).

VI. ANALYSIS

The equations of motion for turbulent boundary-layer flows of a two-component mixture of nonreacting perfect gases are presented, and the procedure for transforming the equations for solution by the implicit finite-difference method used by Anderson and Lewis (Ref. 17) is discussed.

Three eddy viscosity models for specifying the turbulent momentum exchange are presented. The pressure interaction method is developed and the application of the present method is discussed.

6.1 Governing Equations

The governing equations for turbulent boundary-layer flows are given in terms of time averaged, dimensional, physical variables. The substitutions used in nondimensionalizing the equations are presented. The equations used in transforming the governing equations from physical to Levy-Lees variables are given, and the solution procedure is discussed.

6.1.1 Conservation Equations

The conservation equations for two-dimensional, turbulent boundary-layer flows are presented without derivation in terms of mean (time averaged), dimensional, physical variables and are as follows:

Continuity Equation:

$$\frac{\partial \rho u}{\partial x} + \frac{\partial \rho v}{\partial y} = 0 \tag{1}$$

x Momentum Equation:

$$\rho u \frac{\partial u}{\partial x} + \rho v \frac{\partial u}{\partial y} = \frac{\partial}{\partial y} \left[(\mu + \epsilon) \frac{\partial u}{\partial y} \right] \tag{2}$$

y Momentum Equation:

$$\frac{\partial P}{\partial y} = 0 \tag{3}$$

Energy Equation:

$$\begin{aligned} \rho u \frac{\partial H}{\partial x} + \rho v \frac{\partial H}{\partial y} = {} & \frac{\partial}{\partial y} \left[\left(\frac{\mu}{Pr} + \frac{\epsilon}{Pr_t} \right) \frac{\partial H}{\partial y} \right] \\ & + \frac{\partial}{\partial y} \left\{ \left[\frac{\mu}{Pr} (Le - 1) + \frac{\epsilon}{Pr_t} (Le_t - 1) \right] \sum_i h_i \frac{\partial C_i}{\partial y} \right\} \\ & + \frac{\partial}{\partial y} \left\{ \left[\mu \left(1 - \frac{1}{Pr}\right) + \epsilon \left(1 - \frac{1}{Pr_t}\right) \right] u \frac{\partial u}{\partial y} \right\} \end{aligned} \tag{4}$$

Species Equation:

$$\rho u \frac{\partial C_i}{\partial x} + \rho v \frac{\partial C_i}{\partial y} = \frac{\partial}{\partial y} \left[\left(Le \frac{\mu}{Pr} + Le_t \frac{\epsilon}{Pr_t} \right) \frac{\partial C_i}{\partial y} \right] + \dot{w}_i \tag{5}$$

The species equation is specialized for nonreacting gases by setting the production term, $\dot{w}_i$, to zero, and thermal diffusion has been neglected. The conservation equations above are supplemented by the equation of state for each species;

$$p_i = \frac{\rho_i}{m_i} R_o T \tag{6}$$

and by Dalton's law of partial pressures;

$$P = \sum_i p_i \tag{7}$$

Since the mass fractions sum to unity,

$$\sum_i C_i = 1 \tag{8}$$

only one species equation is needed for a two-component mixture. In the present work air is considered as a single species.

In the above equations the viscosity and thermal conductivity are related by the definition of the Prandtl number as below:

$$Pr = \frac{\mu}{k} C_{p_f} \tag{9}$$

where

$$C_{p_f} = \sum_i C_i C_{p_i} \tag{10}$$

In a similar manner the Lewis number is defined by

$$Le = \frac{\rho D_{12}}{k} C_{p_f} \tag{11}$$

For the turbulent exchange processes, turbulent Prandtl and Lewis numbers are defined by the following expressions:

$$Pr_t = \frac{\epsilon}{\kappa} C_{p_f} \tag{12}$$

and

$$Le_t = \frac{\rho D_t}{\kappa} C_{p_f} \tag{13}$$

The eddy viscosity, eddy conductivity and eddy diffusivity are the usual substitutions for the cross-correlation terms which occur in the time averaging of the boundary-layer equations, that is

$$\overline{(\rho v)'u'} = -\epsilon \frac{\partial \bar{u}}{\partial y} \tag{14a}$$

$$\overline{(\rho v)'h'} = -\kappa \frac{\partial \bar{T}}{\partial y} \tag{14b}$$

$$\overline{(\rho v)'C_i'} = -\rho D_t \frac{\partial \bar{C}_i}{\partial y} \tag{14c}$$

The following boundary conditions close the system of equations:

at $y = 0$:

$$u = 0 \tag{15a}$$

$$v = 0 \tag{15b}$$

$$H = H_w \tag{15c}$$

$$\text{or } \left.\frac{\partial H}{\partial y}\right|_w = 0 \tag{15d}$$

$$\left.\frac{\partial C_i}{\partial y}\right|_w = 0 \tag{15e}$$

at $y = y_e$:

$$u = u_e \tag{15f}$$

$$H = H_e \tag{15g}$$

$$\text{and } C_i = C_{i_e} \tag{15h}$$

The condition in Eq. 15b is for a non-porous wall with no mass transfer. If mass transfer through a porous wall were considered as in Ref. 17, this condition would change to

$$v = v_w \tag{15i}$$

The boundary condition at the wall for the energy equation is either for a specified wall temperature (Eq. 15c) or for an adiabatic wall (Eq. 15d). The slot injection wall boundary condition for the species equation is specialized for the present two-component mixture and, with C_i representing the free-stream species, requires a zero net flux of the free-stream species at the wall.

For boundary-layer flows over a flat plate with only the free stream gas present, it is unnecessary to solve the species equation. By omitting the species equation and by setting the laminar and turbulent Lewis numbers to unity, the system of governing equations is reduced to the system of equations for turbulent boundary-layer flows of a single component perfect gas.

6.1.2 Coordinate Transformation

Before solving the boundary-layer equations, the equations were non-dimensionalized as proposed by Van Dyke (Ref. 26) and then transformed using the Levy-Lees variables. In this section, variables which are starred are dimensional and unstarred variables are nondimensional. A reference temperature and a reference viscosity are first defined as

$$T^*_{ref} = U^{*2}_{\infty}/C^*_P \tag{16a}$$

and

$$\mu^*_{ref} = \mu^*(T^*_{ref}) \tag{16b}$$

Using a suitable reference length, L^*, the Van Dyke parameter is defined as

$$\epsilon_{VD}^{\ 2} = \mu^*_{ref}/\rho^*_{\infty}\, U^*_{\infty}\, L^* \tag{16c}$$

the non-dimensional variables are then given by the following relations

$$x = x^*/L^* \tag{17a}$$

$$y = y^*/L^*\ \epsilon_{VD} \tag{17b}$$

$$P = P^*/\rho^*_{\infty}\, U^{*2}_{\infty} \tag{17c}$$

$$\rho = \rho^*/\rho^*_{\infty} \tag{17d}$$

$$T = T^*/T^*_{ref} \tag{17e}$$

$$u = u^*/U^*_{\infty} \tag{17f}$$

and

$$v = v^*/U^*_{\infty}\ \epsilon_{VD} \tag{17g}$$

The resulting nondimensionalized boundary-layer equations were then transformed using the Levy-Lees variables

$$d\xi = \rho_e \mu_e u_e \, dx \tag{18a}$$

and

$$d\eta = \frac{\rho u_e}{\sqrt{2\xi}} dy \tag{18b}$$

The resulting turbulent boundary-layer equations are:

Continuity:

$$2\xi F_\xi + V' + F = 0 \tag{19}$$

Momentum:

$$2\xi FF_\xi + VF' = \beta(\rho_e/\rho - F^2) + \frac{\partial}{\partial\eta}(C(1 + \epsilon^+)F') \tag{20}$$

Energy:

$$2\xi Fg_\xi + Vg' = \frac{\partial}{\partial\eta}\left[\frac{C}{Pr}\left(1 + \frac{\epsilon}{\mu}\frac{Pr}{Pr_t}\right) g'\right]$$

$$+ \frac{\partial}{\partial\eta}\left\{\left[\frac{C}{Pr}\left(Le + \frac{\epsilon}{\mu}\frac{Pr}{Pr_t} Le_t\right) - \frac{C}{Pr}\left(1 + \frac{\epsilon}{\mu}\frac{Pr}{Pr_t}\right)\right] \sum_i \frac{h_i}{H_e} C_i'\right\}$$

$$+ \frac{\partial}{\partial\eta}\left\{\left[C\left(1 + \frac{\epsilon}{\mu}\right) - \frac{C}{Pr}\left(1 + \frac{\epsilon}{\mu}\frac{Pr}{Pr_t}\right)\right] FF'\right\} \frac{u_e^2}{H_e} \tag{21}$$

Species:

$$2\xi FZ_\xi + VZ' = \frac{\partial}{\partial\eta}\left\{\left[\frac{C}{Pr}\left(Le + \frac{\epsilon}{\mu}\frac{Pr}{Pr_t} Le_t\right)\right]\frac{\partial Z}{\partial\eta}\right\} \tag{22}$$

where

$$V = \frac{2\xi}{\rho_e u_e \mu_e}\left[F\frac{\partial\eta}{\partial x} + \frac{(\rho v + \overline{\rho' v'})}{\sqrt{2\xi}}\right] \tag{23}$$

and where $\overline{\rho' v'}$ is the time average of the product of the fluctuating components of the density and normal velocity. The corresponding boundary conditions at the wall, $\eta = 0$, and at the edge of the boundary-layer, $\eta = \eta_e$, for the transformed equations are:

at $\eta = 0$: $\quad F = 0,\ g = H_w/H_e = h_w/H_e$ or $\partial g/\partial\eta = 0$

$$V = V_w,\ \partial Z/\partial\eta = 0 \tag{24}$$

and

at $\eta = \eta_e$: $\quad F = 1,\ g = 1,\ Z = 1$ (25)

6.1.3 Numerical Solution Procedure

The conservation equations in the transformed variables were solved by the implicit finite-difference procedure used in Ref. 17 which requires that the governing equations be written in the general parabolic form

$$W'' + A_1 W' + A_2 W + A_3 + A_4 W_\xi = 0 \tag{26}$$

where W is the dependent variable F, g, or Z and the coefficients A_i are functions of ξ, η, W and W' as given in Ref. 17. When written in the general parabolic form, the momentum, energy and species equations are coupled, non-linear equations and are solved by iteration. At each value of ξ, the iteration continues until F, g and Z at each grid point across the boundary layer change between iterations by less than a specified amount. An alternate convergence test requires that F', g' and Z' at the wall change by less than a specified amount between iterations. For each iteration, the order of solution of the conservation equations is species, energy and momentum; the continuity equation is then solved by trapezoidal integration of the expression

$$V = V_w - \int_0^\eta (2\xi F_\xi + F)\, d\eta \tag{27}$$

6.1.4 Fluid Properties

For a two-component gas mixture in which both components are the same (air injected into air), as considered by Beckwith and Bushnell (Ref. 23) and in the present work, the fluid properties are obtained from standard relations. The density is computed from the equation of state

$$P = \rho R T \tag{28}$$

The viscosity may be computed either from the power law

$$\frac{\mu}{\mu_{ref}} = \left[\frac{T}{T_{ref}} \right]^{0.76} \tag{29}$$

or from Sutherland's formula

$$\frac{\mu}{\mu_{ref}} = \frac{T_{ref} + c^*}{T + c^*} \left[\frac{T}{T_{ref}} \right]^{3/2} \tag{30}$$

where $c^* = 110.3\ ^oK$.

For air mixing with air, Le and $Le_t = 1$, Pr = 0.71 and $Pr_t = 0.90$ were used in this study. Except for the eddy viscosity models which are described in the next section, the fluid properties are complete. By using appropriate fluid properties, injection of a foreign gas (other than air) could be considered. For example, Jaffe, Lind and Smith (Ref. 27) give curve fit data for the enthalpy, specific heat, viscosity and binary diffusion coefficients of argon, helium and carbon dioxide.

6.2. Eddy Viscosity Models

In Eq. 14a above, the turbulent momentum exchange was related to an eddy viscosity. In the present work three eddy viscosity models have been used. Each model has its origin in Prandtl's mixing length concept which is given by the equation

$$\epsilon = \rho \, \ell^2 \left| \frac{\partial u}{\partial y} \right| \tag{31}$$

Two of the models considered are two-layer models which use one expression for the eddy viscosity near the wall and a second expression for the eddy viscosity in the outer portion of the boundary-layer flow. The third is a multi-layer model and uses Eq. 31 all the way across the boundary layer with the definition of ℓ changing in each layer.

6.2.1 Two-Layer Models

Each two-layer model uses the eddy viscosity law of Van Driest (Ref. 28) for the portion of the flow near the wall, but they differ in the eddy viscosity relation used in the outer portion of the flow.

6.2.1.a Van Driest Inner Law

In Ref. 28 Van Driest developed the following expression for the mixing length in terms of physical, dimensional variables:

$$\ell = k_1 \, y \, [1 - \exp(-y^+/A^+)] \tag{32}$$

where $k_1 = 0.4$

$$y^+ = y\rho \, u^+/\mu \tag{33}$$

$$u^+ = (\tau_w/\rho)^{1/2} \tag{34}$$

and for a non-porous wall without pressure gradient $A^+ = 26$. In terms of

physical, dimensional variables, the eddy viscosity for the region of the flow near the wall is given by

$$\epsilon_i^+ = \frac{\epsilon_i}{\mu} = (k_1\ y)^2\ [1 - \exp\ (-y^+/A^+)]^2 \left|\frac{\partial u}{\partial y}\right| \frac{\rho}{\mu} \tag{35}$$

6.2.1.b Clauser Outer Law

The first two-layer eddy viscosity model uses the inner law of Van Driest and an outer law which is based on the work of Clauser. In this outer law the eddy viscosity is given by

$$\epsilon_o^+ = k_2\ \rho\ u_e\ \delta_k^*\ \gamma/\mu \tag{36}$$

where $k_2 = 0.0168$, δ_k^* is the incompressible, two-dimensional boundary-layer displacement thickness and γ is the Klebanoff intermittency factor which is approximated by

$$\gamma = [1 + 5.5\ (y/\delta)^6]^{-1} \tag{37}$$

The Van Driest-Clauser eddy viscosity model has been applied to a variety of problems (see, for example, Refs. 17, 18 and 19), and in the present work this model is applied to the problems of boundary-layer flows over flat plates and flows with tangential slot injection.

6.2.1.c Schetz Outer Law

In the second two-layer eddy viscosity model, the inner law of Van Driest was combined with an outer law proposed by Schetz* in which the Clauser outer law was modified in the slot near region to partially account for effects of slot injection. In the Schetz outer law the eddy viscosity is given by

$$\epsilon_o^+ = \bar{\epsilon}\ \gamma/\mu \tag{38}$$

where γ is the Klebanoff intermittency factor defined above. The variable $\bar{\epsilon}$ is given by one of the two expressions below:

$$\bar{\epsilon} = 0.0168\ \rho\ u_e\ \delta_k^*\ (0) + \frac{\rho_e\ u_e\ x}{730}\left[\frac{1 - \lambda}{1 + \lambda}\right] \tag{39}$$

---

*Private communication with Dr. J. A. Schetz, Chairman, Aerospace Engineering Department, Virginia Polytechnic Institute and State University, Blacksburg, Virginia 24061

or

$$\bar{\epsilon} = 0.0168\ \rho\ u_e\ \delta_k^* \tag{40}$$

where $\delta_k^*(0)$ is the incompressible boundary-layer displacement thickness at the slot lip, x is the distance downstream of the slot and $\lambda = \rho_j u_j / \rho_e u_e$, the ratio of the mass flux from the slot to the mass flux at the edge of the boundary layer. The value of $\bar{\epsilon}$ from Eq. 39 is used at the slot exit and downstream until this value exceeds the value of $\bar{\epsilon}$ from Eq. 40 then $\bar{\epsilon}$ from Eq. 40 is used thereafter. If only the first term of Eq. 39 were used, the outer eddy viscosity would be the Clauser model for the slot lip boundary layer. The use of Eq. 40 gives the standard Clauser outer eddy viscosity for the boundary layer with slot injection. In general, δ_k^* is larger than $\delta_k^*(0)$ and the inclusion of the second term in Eq. 39 provides a transition from the value of the outer eddy viscosity model for the slot lip boundary layer to that of the boundary layer with slot injection.

6.2.2 Multi-Layer Model

The multi-layer eddy viscosity model is that proposed by Beckwith and Bushnell (Ref. 23) in which the eddy viscosity model used in Ref. 16 is modified for tangential slot injection. The eddy viscosity model used for fully developed turbulent boundary-layer flow and the model modified for tangential slot injection are presented. It is convenient to first rewrite Eq. 31 incorporating the Van Driest damping function in the basic expression for ϵ since this term is effective only quite near the wall in the so-called laminar sub-layer. Rewriting Eq. 31 as indicated gives

$$\epsilon^+ = \ell^2\ [1 - \exp\ (-y^+/A^+)]^2\ \left|\frac{\partial u}{\partial y}\right|\ \frac{\rho}{\mu} \tag{41}$$

Subsequent attention is restricted to specifying the mixing length, ℓ.

6.2.2.a Mixing Length for Fully Developed Turbulent Flow

For fully developed turbulent boundary-layer flows, the mixing length is defined in three layers. Values of y and ℓ are given at three points in the boundary layer, and these points are connected by straight line segments. These "pivot points" and the corresponding values of y and ℓ are:

Point	y/δ	ℓ	
0	0	0	
1	0.1	$0.1K\delta$	(42)
2	0.3	$\tilde{f}\delta$	

and for $y > 0.3\delta$, $\ell = \tilde{f}\delta$, where $K = 0.4$ and $\tilde{f}$ is given by

$$\tilde{f} = 0.265 - 0.196\, H_k^* + 0.0438\, H_k^{*2} \tag{43}$$

where $H_k^* = \delta_k^*/\theta_k$ and θ_k is the incompressible boundary-layer momentum thickness. This model gives the same eddy viscosity near the wall as does the Van Driest-Clauser model and differs only in the outer portion of the flow.

6.2.2.b Modified Mixing Length for Tangential Slot Injection

For tangential slot injection, three distinct zones in the flow field are considered, and in each zone, the mixing length pivot point coordinates are different. The boundaries of the zones are determined from the relative values of the mixing length in the slot flow region, ℓ_j, in the mixing region, $\ell_{u,m}$, and in the outer flow field, ℓ_b.

For the slot flow region, ℓ_j is constant and is given by

$$\ell_j = a_j\, s/2 \tag{44}$$

where s is the slot height and a_j is a constant. Ref. 23 gives $a_j = 0.14$ for turbulent slot flow.

For the mixing region, $\ell_{u,m}$ is given by

$$\ell_{u,m} = a_m\, W\, Pr_t/Le_t \tag{45}$$

where W is the width of the mixing zone between the slot flow and the outer flow and a_m is a constant. The values of a_m (see Ref. 23) should be in the range of 0.05 to 0.12, with 0.09 being the recommended value. With the normalized species concentration, $\tilde{Z}$, is given by

$$\tilde{Z} = (C_i - C_{i,w})/(C_{i,e} - C_{i,w}) \tag{46}$$

then W is defined by

$$W = y_f - y_n \tag{47}$$

where $y_f = y$ at $\tilde{Z} = 0.99$ and $y_n = y$ at $\tilde{Z} = 0.01$.

In the outer flow field, the mixing length is given by

$$\ell_b = \tilde{f}_s(\delta - y_n) \tag{48}$$

For tangential slot injection, $\tilde{f}_s$ has the same form as $\tilde{f}$ in Eq. 43 with H_k^* being replaced by $H_{k,s}^*$ where $H_{k,s}^* = \delta_{k,s}^*/\theta_{k,s}$. The subscript s denotes that the limits of integration for the incompressible displacement and momentum thicknesses is changed from y_n to δ instead of 0 to δ. These limits of integration were recommended by Beckwith and Bushnell (Ref. 23) for tangential slot injection.

With ℓ_j, $\ell_{u,m}$ and ℓ_b defined, the three zones can be specified. In each zone, pivot points and corresponding coordinates for y and ℓ are given, and the mixing length distribution is obtained by connecting the coordinate points with straight line segments. A schematic representation of a flow field with tangential slot injection is given in Fig. 1 with appropriate representations of velocity, species concentration and mixing length profiles.

<u>Zone I</u> (Initial Mixing Region) is defined by the inequality

$$\ell_j \geq \ell_{u,m} < \ell_b \tag{49}$$

and the pivot points and the coordinates of y and ℓ are:

Point	y	ℓ
0	0	0
1	$\frac{s}{2K} a_j$	$\frac{s}{2} a_j$
2	$s(1 - \frac{a_j}{2K}) \frac{\delta}{\delta_r}$	$\frac{s}{2} a_j$
3	y_m	$\frac{Pr_t}{Le_t} a_m W$
4	$(s + t + \frac{\tilde{f}_s \delta_o}{K}) \frac{\delta}{\delta_r}$	$\tilde{f}_s(\delta - y_n)$

(50)

where s is the slot height, t is the lip thickness, y_m = y at $\tilde{Z} = 0.5$, δ_o is the thickness of the boundary-layer above the lip, and $\delta_r = \delta_o + t + s$.

Zone II (Intermediate Mixing Region) is defined by the inequality

$$\ell_j \le \ell_{u,m} \le \ell_b \tag{51}$$

and the coordinates of the pivot points are given by the following values:

Point	y	ℓ
0	0	0
1	$\frac{Pr_t}{Le_t}\frac{a_m}{K}W$	$\frac{Pr_t}{Le_t}a_m W$
3	y_m	$\frac{Pr_t}{Le_t}a_m W$
4	$(s + t + \frac{\tilde{f}_s\delta_o}{K})\frac{\delta}{\delta_r}$	$\tilde{f}_s(\delta - y_n)$

(52)

In Zone II one less pivot point is needed than in Zone I and point 2 is dropped.

Zone III (Approach and Relaxation to Equilibrium Boundary Layer) is specified by the relation

$$\ell_j \le \ell_{u,m} \ge \ell_b \tag{53}$$

and the coordinate of the pivot points are:

Point	y/δ	ℓ
0	0	0
1	0.1	$0.1K\delta$
4	0.3	$\tilde{f}_s\delta$

(54)

In Zone III, the mixing length distribution is the same as was given for fully developed turbulent boundary-layer flow in Section 2.2.a above with the exceptions of the labeling of the outer pivot point and the use of $\tilde{f}_s$ instead of $\tilde{f}$. Beckwith and Bushnell suggest that the boundary of Zone III may alternately be taken as that value of x at which the concentration of the free stream species at the wall exceeds 85 percent, i.e.

$$C_{air,w} \ge 0.85 \tag{55}$$

In the present method, relations (53) and (55) are both used, and Zone III is initiated when either inequality is first satisfied.

6.3 Pressure Interaction Effects

In the present finite-difference method, the static pressure at the edge of the boundary layer can either be constant as for flow over a flat plate or the pressure can have a varying distribution as for flow in a nozzle. Further, it is possible to consider flows over flat plates which do not have constant edge static pressure as might be the case in a wind tunnel if the pressure varied along the test section.

In flows with tangential slot injection, if the slot and freestream static pressure are matched, the static pressure along the boundary-layer edge will be nearly constant. However, if the slot pressure is lower than the freestream pressure, the edge pressure distribution will show an expansion zone immediately downstream of the slot and a recovery to the freestream static pressure as the distance downstream of the slot increases. Ideally, this pressure distribution should be the same as that for isentropic, inviscid flow over an effective body whose shape corresponds to the boundary-layer displacement thickness. In computing a pressure distribution from the boundary-layer displacement thickness distribution, a coupling or interaction effect occurs, i.e., changing δ^* changes P and vice versa. Thus, an iterative procedure is required for determining displacement thickness-pressure interaction effects.

In the present finite-difference method, such an iterative procedure for pressure interaction effects has been included as an option. The present pressure interaction method is a global iteration procedure in that a calculation is first made with an initial pressure distribution, a distribution is computed from the calculated displacement thickness distribution, and a new boundary-layer calculation is made using a pressure distribution which is a combination of the initial distribution and the pressure distribution computed from the displacement thickness. This iterative procedure is continued until the change in the pressure distributions between iterations is sufficiently small. Twelve to fifteen iterations usually give a maximum change in pressure between iterations of about 0.2 percent.

In the pressure interaction method, it is assumed that the flow is isentropic and that Prandtl-Meyer theory is applicable. From the displacement thickness slope, $d\delta^*/dx$, a value of the Mach number, M, is obtained using Prandtl-Meyer theory, and P/P_o is calculated using isentropic flow equations. Denoting the

pressure distribution used for the last iteration by P_{old}, the pressure distribution computed from δ^* by P_{δ^*}, and the pressure distribution to be used for the next iteration by P_{new}, then P_{new} is given by

$$P_{new} = P_{old} (1 - w) + w P_{\delta^*} \tag{56}$$

where w is a weighting factor. Since the interaction between the pressure distribution and the displacement thickness can be fairly strong, w should be kept small so that the interaction procedure will be stable. Values of w which have been used have been 0.05 to 0.20. If no major instability tendencies exist for a particular set of conditions, it is possible to use w = 0.20. If, however, maintaining stability is a problem, w should be reduced; to 0.05 if necessary.

Since the distribution of δ^* may not be smooth, especially in the region near the starting point, $d\delta^*/dx$ is obtained from a six point walking least squares log-log curve fit. This curve fit procedure provides a smoother derivative of δ^* than would be obtained using a three or four point Lagrangian interpolating polynomial. In general, the value of x at which a solution is obtained and at which P_{new} is calculated are not the same as the input values of x corresponding to the initial or input pressure distribution. Values of P_{new} are obtained at input values of x using the six point walking least squares log-log curve fit for interpolation.

For low pressure slot injection, pressure interaction calculations can be started at the slot exit or downstream of the exit if necessary. If the calculation is begun at the slot exit, the initial pressure distribution is taken to be the flat plate (no slot) constant static pressure. The final calculated pressure distribution will show a drop from the freestream pressure downstream of the slot exit and a subsequent recovery to the freestream pressure. Results obtained with the pressure interaction method starting at the slot exit indicate that reasonable agreement with experimental data can be expected when adequate experimental data are available for comparison.

If pressure interaction calculations for low pressure injection are started downstream of the slot exit within the expansion region, a constant initial pressure distribution cannot be used. The expansion and subsequent recompression would not be properly predicted. In such a case, it is desirable to construct an initial pressure distribution which starts with the experimental pressure value

in the expansion region and has a transition to the freestream pressure value downstream. In addition, dummy values of x, P and δ^* are specified for values of x upstream of the starting point of the calculation. These points provide a constant pressure and an upstream slope for δ^* which corresponds to the amount that the flow has expanded from upstream of the slot to the point where the calculation is started. This procedure has been used for one set of conditions, and the final calculated pressure distribution agreed well with the experimental pressure data.

The present interaction method has not been applied to cases of high pressure injection for which an initial pressure distribution similar to that described in the above paragraph should be used. The initial pressure distribution should start at the slot with the pressure which occurs at the slot exit and decreases to the freestream pressure at some appropriate downstream point. This pressure distribution would correspond to a hypothetical situation in which the flow had undergone a compression prior to the point where the calculation was started and would then subsequently expand to the freestream pressure.

6.4 Application of Finite-Difference Method

The application of the present finite-difference method is very similar to the application of the method described in Ref. 17. The grid spacing in the normal and streamwise directions is controlled in the same way. For flow over a flat plate the same starting profiles are used, i.e.

$$\frac{u}{u_e} = 1 - e^{-\eta} \tag{57}$$

and

$$\frac{H}{H_e} = \frac{H_w}{H_o} + \left(1 - \frac{H_w}{H_o}\right) \frac{u}{u_e} \tag{58}$$

and a calculation is started at x = 0 if the flow is laminar and at x = 0.0001 if the flow is fully turbulent.

For calculation of flows with tangential slot injection, it is necessary to provide initial velocity, enthalpy and species concentration profiles. In order to avoid the small recirculation region which occurs immediately behind the slot lip, the calculation should be started no closer to the slot than two lip thicknesses. Initial profiles for velocity and enthalpy might be obtained from

experimental data or if adequate experimental data are unavailable, initial profiles might be synthesized by combining results of a flat plate finite-difference prediction for the portion of the profiles above the slot lip with a reasonable approximation for slot flow profile. The accuracy of the results of the calculations will be dependent upon the appropriateness of the initial profiles. For maximum effectiveness of the finite-difference method as a predictive technique, it is desirable to use the minimum of experimental data, whereas, to obtain the best accuracy possible with the finite-difference method, it is desirable to use available experimental data where appropriate, as for the initial profiles.

For calculations of flows with tangential slot injection, it is necessary to start the calculation with a value of $\xi > 0$. In using the present method, an initial or starting value of ξ was determined by matching the displacement and momentum thicknesses of the slot lip boundary layer with the parameters obtained from a calculation of flow over a flat plate at the test conditions. It is not necessary to obtain an exact match for both δ^* and θ since the calculated results are not strongly affected by the initial value of ξ.

In the present method, either wall or local flow properties can be used in the Van Driest damping function, $[1 - \exp(-y^+/A^+)]$. If local properties are used, Eqs. 33 and 34 remain unchanged and y^+ is given by

$$y^+ = y\rho u^+/\mu \tag{33}$$

where

$$u^+ = (\tau_w/\rho)^{1/2} \tag{34}$$

If, however, wall properties are used, the expressions for y^+ and u^+ change to

$$y^+ = y\rho_w u^+/\mu_w \tag{59}$$

and

$$u^+ = (\tau_w/\rho_w)^{1/2} \tag{60}$$

Most finite-difference methods for predicting turbulent boundary-layer flows which have used the Van Driest damping factor in the eddy viscosity expressions have evaluated ρ and μ locally. However, recent investigations of Bushnell and Morris (Ref. 29) indicate that for some test conditions, Eqs. 59 and 60 should be used instead of Eqs. 33 and 34, i.e., the flow properties in the Van Driest damping function should be evaluated at the wall.

VII. RESULTS AND DISCUSSION

Calculations have been made with the present finite-difference method for two sets of data for supersonic flows with tangential slot injection; the experimental data and the finite-difference predictions of Cary (Ref. 21) and the experimental data of Kenworthy and Schetz (Ref. 30).

7.1. Cary's Slot Injection Experimental Conditions

In Ref. 24, Cary and Hefner reported the results of a series of experiments in which air was tangentially injected into a Mach 6 turbulent boundary layer. Also presented in Ref. 24 are finite-difference predictions for six of the experimental cases using the method of Ref. 23. In the experimental investigation, three slot heights were considered (s = 0.158 cm, 0.475 cm and 1.116 cm or 1/16, 3/16 and 7/16 in), and for each slot height the total enthalpy of the slot flow was varied over a range of values. Additionally, the mass flow from the slot, λ, was varied from 0.0165 to 1.6. For these mass-flow rates, the ratio of wall static pressure with slot injection to wall static pressure without the slot present, $P_w/P_{w,o}$, ranged from $P_w/P_{w,o} \simeq 0.3$ to $P_w/P_{w,o} \simeq 2.8$. The finite-difference predictions given in Ref. 24 were for $P_w/P_{w,o} \simeq 1.0$, and were made using initial velocity and total enthalpy profiles obtained from the experimental data. The initial species concentration profiles used by Cary were modified step functions with some smoothing of the step corners.

An initial value of ξ was determined by making calculations for flow over a flat plate using the Ref. 24 test conditions. In these calculations, the Van Driest-Clauser and the Beckwith-Bushnell eddy viscosity models were used with both wall and local properties in y^+. The experimental values of δ, δ^*, and θ were closely matched at x = 470 cm (185 in) on the flat plate and the corresponding value of ξ was used in the calculations of flow with slot injection. The skin-friction distributions predicted by these calculations are shown in Fig. 2 for the portion of the plate downstream of the slot location, i.e. x = 470 to x = 508 cm (185 to 200 in) or x = 0 to x = 38.1 cm (15 in) downstream of the slot location. Good agreement was obtained with the experimental data of Cary, especially using the Beckwith-Bushnell ϵ^+ with wall properties in y^+. Changing from wall to local properties in y^+ changed the predictions of C_f by less than 1 percent, and changing the eddy viscosity models changed the predictions

of C_f by about 3 percent. The agreement between the experimental and predicted skin friction further justifies the assumption of the slot location.

Calculations for the six matched pressure cases of Cary were made with a constant static pressure distribution, neglecting pressure interaction effects, and the predicted skin-friction distributions were compared with the experimental data and with the finite-difference predictions of Cary. Tabulations of the initial profiles used by Cary were obtained (by private communication), and these profiles were used for the slot injection calculations. Values of η were calculated corresponding to the values of y in the initial profile data, and linear interpolation was used to obtain the profile values at the grid points used in the present finite-difference method.

The predicted skin-friction distributions for Cary's Cases I through VI are shown in Fig. 3. The Beckwith-Bushnell eddy viscosity model was used, and both wall and local properties were used in y^+. Also shown for each case is the predicted C_{f_o} (flat plate) distribution, and the experimental skin-friction distributions obtained by Cary.

When wall properties were used in y^+, the results predicted by the present method consistently agreed well with the results of the calculations Cary made with the method of Ref. 23 using wall properties in y^+. However, if local properties were used in y^+, the predicted C_f was consistently 10 percent higher than the results of Cary, and the predicted C_f approached more rapidly the flat plate value C_{f_o}. For these cases, predictions of drag reduction were strongly influenced by the choice of flow properties in the Van Driest damping function.

Calculations were also made for Case V using the Van Driest-Clauser and the Van Driest-Schetz eddy viscosity models. The skin-friction distributions predicted with these models are shown in Fig. 4 and are compared with the results of the Beckwith-Bushnell eddy viscosity model and the experimental data of Cary. At 34 slot heights downstream of the slot, the Van Driest-Clauser model results were only 3.5 percent higher than the Beckwith-Bushnell ϵ^+ results, and the Van Driest-Schetz eddy viscosity model results were about one or two percent lower than the results obtained with the Van Driest-Clauser model. For each eddy viscosity model, using local instead of wall properties in y^+ increased C_f by about 10 percent. These results indicate that the Van Driest-Clauser and Van Driest-Schetz eddy viscosity models can be used reasonably in prediction of

boundary-layer flows with tangential slot injection and can be expected to give a slightly more conservative prediction of drag reduction than the Beckwith-Bushnell eddy viscosity model.

Calculations were also made with the effects of pressure interaction included. These calculations were for Cary's Case V and for a similar case with the slot mass flow rate, λ, reduced from 0.047 to 0.0165. The lower value of λ corresponds to the lowest mass flux considered in Ref. 24 for s = 1.11 cm (7/16 in). The initial profiles for $\lambda = 0.0165$ were obtained by using the Case V total enthalpy and species concentration profiles and the free-stream portion of the velocity profile. The slot portion of the Case V velocity profile was scaled so that the integrated mass flux for the slot portion of the profile was 0.0165. The two portions of the velocity profile were joined and smoothed with a four point walking least squares log-log curve fit. The initial velocity profiles for $\lambda = 0.0165$ and for Cary's Case V are shown in Fig. 5. The integrated slot mass flux for Case V was 0.054, and this value is indicated in Fig. 5 as is Cary's experimental value of 0.047.

The predicted skin-friction distributions, with and without pressure interaction, for $\lambda = 0.0165$ and 0.054 are shown in Fig. 6. Also shown are the experimental results of Cary. For these calculations, the Beckwith-Bushnell eddy viscosity model was used with wall properties in y^+. Except near the slot, the predicted skin-friction distributions with and without pressure interaction differed by 7 percent or less. The predicted pressure distributions for $\lambda = 0.054$ and 0.0165 are shown in Fig. 7 as is the flat plate pressure. For $\lambda = 0.054$, the predicted pressure distribution differed from the flat plate pressure by about 8 percent, and for $\lambda = 0.0165$, the predicted reduction in pressure was about 20 percent. The predicted pressure distributions appear to agree fairly well with the experimental wall pressure data of Cary, but the experimental data given in Ref. 24 for these mass flow rates were sparse and could not be extracted with sufficient confidence to justify inclusion in Fig. 7.

The skin-friction distributions do show some effect of the predicted pressure gradients, but the pressure gradients predicted are not large enough to have a strong influence on the predicted C_{f_∞} distributions. In fact, for Cary's matched and low pressure injection conditions, pressure interaction had a smaller effect on the predictions of skin-friction than did changing eddy viscosity models or changing from wall to local flow properties in y^+.

7.2. Kenworthy and Schetz Slot Injection Experimental Conditions

In the experiments conducted at the Virginia Polytechnic Institute and State University by Kenworthy and Schetz, air was tangentially injected through an 0.635 cm (0.25 in) slot into a Mach 2.4 turbulent boundary layer. Two mass flow rates were considered; for the higher mass flow rate the Mach number of the slot flow was $M_j = 0.66$ and for the lower mass flow rate $M_j = 0.31$. For both values of M_j, the total temperature of the slot and freestream flows were the same. For $M_j = 0.66$ (matched pressure injection), the wall pressure distribution was nearly constant and was equal to the pressure for $M = 2.37$. For the low pressure, $M_j = 0.31$, the wall static pressure dropped about 20 percent at the slot and recovered to the freestream value in about eighteen slot heights.

Because no experimental data were available for the flat plate or no-slot conditions, an initial value of ξ was obtained by matching values of δ^*, θ, and δ from calculations of flow over a flat plate at the test conditions with values from previous calculations which had been made for flow in the nozzle before it was modified for the slot injection experiments. The location of the slot in the nozzle test section was known. The values of δ^*, θ, and δ at the slot location in the nozzle boundary-layer flow were reasonably matched with the corresponding values for the flat-plate boundary layer at 63.5 cm (25 in) from the leading edge of the flat plate. The corresponding value of ξ was used in the subsequent calculations of flow with tangential slot injection. The predicted distributions of the wall shear stress on the flat plate downstream of the slot location are shown in Fig. 8. The values of τ_w predicted with the Beckwith-Bushnell eddy viscosity model were about 2 percent higher than the values predicted with the Van Driest-Clauser model. Wall or local properties in y^+ affected the predicted values of τ_w by 2 or 3 percent.

The eddy viscosity profiles for the flow over the flat plate at the slot location are shown in Fig. 9. Near the wall the two models had the same representation and gave nearly the same value of the eddy viscosity. A higher peak value of ϵ^+ was given with the Beckwith-Bushnell model than with the Van Driest-Clauser model, but near the outer edge of the boundary layer the eddy viscosity went to zero more sharply than with the Van Driest-Clauser model. In the Clauser outer law ϵ^+ was driven to zero by the Klebanoff intermittancy factor, and in the Beckwith-Bushnell model ϵ^+ went to zero as du/dy tended to zero.

Initial profiles for the slot injection calculations were obtained from the experimental data. Total pressure profiles were measured at Stations 1, 2, 3 and 4 (2.22, 7.62, 12.7 and 17.78 cm or 0.875, 3, 5 and 7 in downstream of the slot), but experimental profiles were not measured at the slot exit. The calculations were started at x = 2.22 cm (0.875 in) using initial profiles derived from experimental data. Curves were faired through the experimental Station 1 Mach number profiles. From these curves additional points were taken, and, assuming a constant total enthalpy profile ($H/H_e = 1.0$), corresponding values of u/u_e were calculated. A species concentration profile was obtained from

$$Z = C_i/C_{i_e} = 1/\{1 - \exp[-100\,(y-y_p)]\} \tag{61}$$

where y_p is the value of y at which Z = 0.5, and y_p was taken to be the slot height, $y_p = s = 0.635$ cm (0.25 in).

Using these initial profiles and the Beckwith-Bushnell eddy viscosity model with wall properties in y^+, calculations were made neglecting pressure interaction effects, for both the matched and low pressure injection cases. For matched pressure injection, the experimental pressure distribution was nearly constant, and a constant pressure (corresponding to M = 2.4) was used in the calculations. For the low pressure injection case, a curve was faired through the experimental wall pressure values (as shown in Fig. 10), and this pressure distribution was used in the calculations for low pressure injection. The predicted wall shear distributions are shown in Fig. 11 with the experimental data of Kenworthy and Schetz and the predicted flat-plate wall shear distribution. For both matched and low pressure injection, a reduction in wall shear was predicted. Near the slot exit, a greater reduction in wall shear was predicted with low pressure injection, but, further downstream, the greater reduction in wall shear was predicted for matched pressure injection. For matched pressure injection, good agreement was obtained with the experimental data. The present method slightly underpredicted the wall shear at Station 2 and equally overpredicted the wall shear at Stations 3 and 4. For low pressure injection, the predicted wall shear agreed reasonably well with the experimental value at Station 2, but agreed poorly at Stations 3 and 4. The lack of agreement between experiment and prediction was not unexpected for the low pressure injection case since the experimental value of τ_w at Station 3 was equal to the predicted flat plate (no slot) value and was about 40 percent higher at Station 4. The trends of the predicted

wall shear or skin-friction distributions for the Cary cases and for the Kenworthy and Schetz cases seemed consistent, whereas the experimental values of τ_w for the low pressure injection case of Kenworthy and Schetz did not fit the trends of the other experimental data.

Predicted and experimental Mach number profiles at Stations 1-4 are shown in Fig. 12 for low pressure injection and in Fig. 13 for matched pressure injection. Reasonable to good or excellent agreement was obtained between the experimental and predicted profiles. At Station 1 the predicted profiles were for x = 2.35 cm (0.925 in), the first value of x downstream of the initial value at which a finite-difference solution was obtained. For low pressure injection, the predicted profiles agreed well with the experimental profiles. For matched pressure injection, the agreement between experiment and prediction was not as good and poorer agreement was obtained at Stations 3 and 4 than at Station 2.

Predicted and experimental pitot pressure profiles are shown in Figs. 14 and 15. For low pressure injection, the edge of the experimental boundary layer was assumed to be at y = 1.52 cm (0.6 in), and the experimental data were normalized by the pitot pressure at y = 1.52 cm rather than the free-stream pitot pressure. The agreement between the experimental and predicted pitot pressure profiles was the same as for the Mach number profiles. The overpredictions of Mach number and pitot pressure for the inner part of the boundary layer for the matched pressure injection case appears to be consistent with the interpretation of schlieren photographs of the flow. The schlieren photographs indicate that the turbulence level in the inner portion of the boundary-layer flow (except perhaps very near the wall) was considerably lower than the level of turbulence in the outer portion of the flow, while the eddy viscosity model used assumes essentially fully turbulent flow throughout the boundary layer.

Calculations were also made for the matched pressure injection case with the other eddy viscosity models. Fig. 16 shows the predicted wall shear distribution with all three eddy viscosity models using both local and wall properties in y^+. The choice of local or wall properties affected the predictions of τ_w by about 2 percent, while use of the Van Driest-Clauser model gave predictions of τ_w about 10 percent higher than the Beckwith-Bushnell model. The predictions of τ_w with the Van Driest-Schetz model were about one percent lower than with the Van Driest-Clauser model and are not separately shown. The Mach number profiles predicted

are shown in Figs. 17-20. Changing the eddy viscosity models had only slight effect on the predictions of Mach number, and there were no plottable differences based on choice of local or wall properties in y^+.

Calculations were also made for the matched pressure injection case with the Beckwith-Bushnell eddy viscosity model with wall properties in y^+ and with different values of a_j and a_m. In the finite-difference method, whether the slot flow is laminar or turbulent is controlled by a_j, and whether the mixing of the slot and freestream flows is laminar or turbulent is controlled by a_m. As noted above, schlieren photography of the flow indicated the inner portion of the flow may have been less than fully turbulent and the values of $a_j(0.14)$ and $a_m(0.09)$ which were used were the values recommended in Ref. 23 for turbulent boundary-layer flow. In fact, Ref. 23 gave a range of values for $a_m = 0.005$ to 0.12. Six calculations were made with $a_j = 0.14$ and 0.014 and with $a_m = 0.09$, 0.05 and 0.01, and the predicted results are shown in Figs. 21-25. In Fig. 21 the predicted distributions of wall shear are shown. Reducing either a_j or a_m reduced the predicted wall shear, and, except for $a_m = 0.01$, the change in a_j had a smaller effect of the predictions of τ_w than did the changes in a_m.

Near the wall the changes in a_j and a_m affected the predictions of the Mach number profiles shown in Figs. 22-25, but had only a small effect on M from $y = 0.635$ cm (0.25 in) outward. For $y/s < 1$, some of the assumed values for a_j and a_m improved the agreement between the predicted and experimental Mach number profiles, but from $y/s = 1$ to 2 the agreement was not improved. The best prediction of Mach number profiles was obtained with $a_j = 0.14$ and $a_m = 0.01$ which corresponds to turbulent slot flow and laminar mixing. With these values of a_j and a_m, the prediction of τ_w was consistently below the experimental data, but the agreement between experiment and predictions of τ_w was still as good as with $a_j = 0.14$ and $a_m = 0.09$. The results obtained with $a_j = 0.14$ and $a_m = 0.01$ indicated that still better agreement might be obtained if the predicted mixing region were moved further out in the flow. Calculations were made with values of 0.762 and 0.889 cm (0.30 and 0.35 in) for y_p (see Eq. 61). The prediction of τ_w was not affected by a plottable amount, and only small differences in the Mach number profiles were obtained. The greatest differences in the profiles occurred at Station 4 as shown in Fig. 26. No significant improvement between experiment and finite-difference prediction was obtained. The comparison between the experimental data of Kenworthy and Schetz and the predictions of the present finite-

difference method did not give as good agreement as might have been expected. For low pressure injection, good agreement was obtained for the profile data, but the agreement in the wall shear data was not as good. The converse applied for matched pressure injection; good agreement was obtained for the wall shear data, but the agreement for the profile data was not as good.

Additional experimental data and theoretical predictions are needed to explain the differences in the profile and wall shear data observed. The effects of additional factors affecting the experiment which were not included in the theoretical model (e.g. the apparent wake from the splitter plate) and the influence of experimental error in the Station 1 profile data on the predictions of the downstream profiles should be further investigated.

Calculations were also made for the low pressure injection case with the effects of pressure interaction included. The predicted wall shear is shown in Fig. 27 as is the predicted wall shear from Fig. 11 which used the experimental pressure distribution and a wall shear distribution from a calculation with constant pressure (M = 2.4). The wall shear predicted with pressure interaction was almost exactly the same value as predicted using the experimental pressure distribution, and was lower than the wall shear predicted for constant pressure. The same results were found previously for the Cary cases (see Fig. 6). As also noted the effects of pressure interaction were smaller than the effects of changing eddy viscosity models.

For the Cary slot injection cases, comparison between experimental and predicted pressure distributions was not possible, but such comparisons could be made for the Kenworthy and Schetz low pressure injection case. The experimental and predicted pressure distributions are shown in Fig. 28. The agreement was very good and the present method correctly predicted the pressure distribution throughout the interaction region.

7.3. Computing Time Required

The calculations with the present finite-difference method discussed in the previous two sections were run on the IBM 370/155 system of the Virginia Polytechnic Institute and State University's Computing Center. Representative computing times for the Cary Case V conditions are shown in Table I below:

TABLE I. Computing Times for Cary Case V Conditions

Eddy Viscosity Model	Gas Model	Convergence Criterion (percent)	Total Number of Iterations	Time (Min:Sec)
Beckwith-Bushnell	Binary	10	105	4:01
Van Driest-Clauser	Binary	10	85	3:27
Van Driest-Clauser	Perfect	10	72	1:55
Van Driest-Schetz	Perfect	10	72	2:05
Van Driest-Schetz	Perfect	1	92	2:21

For these calculations, the convergence test required that each of the velocity, enthalpy, and species concentration profiles at each point across the boundary layer changed by less than the indicated percentage. With the Beckwith-Bushnell eddy viscosity model, it is necessary to solve the species conservation equation as well as the energy and momentum equations and the gas mixture was a two-component binary gas. For the Van Driest-Clauser and the Van Driest-Schetz eddy viscosity models, the gas model can be either a two-component mixture or a single component perfect gas. The predictions of skin friction were affected by about two percent by changing gas models. The binary gas model required more iterations (to obtain convergence for the species equation) than did the perfect gas model and differences of about two percent in predictions of skin friction are to be expected.

The data given in Table I show that for a binary gas the computing time with the Van Driest-Clauser eddy viscosity model was fourteen percent less than with the Beckwith-Bushnell model, and that the computing time for a one component gas with the Van Driest-Clauser model was less than one half of the time required with the Beckwith-Bushnell model and a binary gas. Also, the computing times for the calculations with the Van Driest-Clauser model and the Van Driest-Schetz model were nearly the same. Further, it is shown that requiring one percent instead of ten percent convergence increased the computing time by about thirteen percent and had negligible effect on the prediction of skin friction. For these calculations the surface length considered was 38.1 cm (15 in).

Representative computing times for the VPI conditions for the matched pressure injection case are given in Table II below.

TABLE II. Computing Times for VPI Conditions

Eddy Viscosity Model	Total Number of Iterations	Time (Min:Sec)
Beckwith-Bushnell	150	5:26
Van Driest-Clauser	122	4:38
Van Driest-Schetz	122	4:32

For these calculations, the binary gas model was used, the convergence criterion was one percent and the surface considered was from 2.22 to 38.1 cm (0.875 to 15 in) downstream of the slot. The trends are the same as for the Cary conditions with more computing time required when considering the gas as a binary mixture and when using the tighter convergence criterion (one percent).

For the pressure interaction calculations, the convergence criteria were ten percent for the Cary conditions and one percent for the VPI conditions. Fifty-five minutes of computing time were allowed and twelve to fourteen global iterations were completed in that time.

For all calculations considered, 100 points across the boundary layer were used with a value of 1.09 for the spacing parameter (see section 6.2.3 of Ref. 17). Solutions were obtained at about 40 values of x with a minimum of two iterations at each value of x. The starting value of x was 0.127 cm (0.05 in) and Δx was limited to 1.27 cm (0.5 in).

In the present work, the function test was used for all of the calculations. For the Cary conditions, the convergence criterion was ten percent, the perfect gas model was used with the Van Driest-Clauser and the Van Driest-Schetz eddy viscosity models and the two-component gas model was used with the Beckwith-Bushnell eddy viscosity model. For the VPI conditions, a one percent convergence criterion was used and the calculations were with the binary gas model. Calculations were also made with the derivative convergence test and one percent convergence criterion. The computing times required, number of iterations and predictions of these calculations were essentially the same as the calculations with a ten percent function convergence test.

VIII. CONCLUSIONS

In the present work, a finite-difference method has been developed for the prediction of boundary-layer flows with tangential slot injection with the effects of pressure interaction included. Previous methods applicable to tangential slot injection which predicted wall-measurable properties did not include the effects of pressure interaction (for example Beckwith and Bushnell (Ref. 23)), or, if pressure interaction effects were included, wall-measurable properties were not predicted (e.g. Kurkov (Ref. 25)). Predictions of wall skin-friction and wall static pressure distributions obtained with the present method generally agreed well with the available experimental data.

Some significant differences between the experimental data of Kenworthy and Schetz and the results of the present finite-difference method were observed in profile and wall shear data. Further experimental data and theoretical predictions are needed to explain these differences. Additional mass flow rates should be considered. For further theoretical studies, experimental data for the flat-plate (no slot) conditions are needed as are complete wall and profile data at the slot exit. For the Cary conditions, experimental profile data at locations other than the slot exit would have greatly enhanced the comparison between experimental results and finite-difference predictions. In particular, the arbitrary factors in the Beckwith-Bushnell eddy viscosity model (viz. a_j, a_m and the choice of wall or local properties in the "Law of the Wall" region) could perhaps have been specified with more confidence.

Previous finite-difference methods which were used to predict turbulent boundary-layer flows with tangential slot injection considered only one eddy viscosity model. In the present work, three eddy viscosity models have been considered, and the results obtained with each model were in good agreement with the available experimental data. For prediction of wall-measurable quantities far downstream of the slot, the Van Driest-Clauser model can be recommended because of its simplicity and because the results obtained with it agreed well with experimental data. The Beckwith-Bushnell model is recommended in the slot near region despite its greater complexity because (i) the results obtained with this model agreed better with experimental data than did the results obtained with the Van Driest-Clauser model, (ii) this model contains constants which can be adjusted to represent laminar or turbulent mixing of the slot and freestream flows

and (iii) this eddy viscosity model can be used for laminar or turbulent slot flow. The results obtained with the Van Driest-Schetz eddy viscosity model were in better agreement with the available experimental data by about one percent than the results with the Van Driest-Clauser model. The Van Driest-Schetz model is only slightly more complicated than the Van Driest-Clauser model and the computing times are equivalent. Unless the flow field for less than about thirty slot heights is of principal interest, the eddy viscosity law of choice for injection of air into air would be the Van Driest-Clauser model with a perfect (one-component) gas model since (i) the computing time required is less than one half of the time required with the Beckwith-Bushnell model, (ii) the Van Driest-Clauser model is significantly less complicated than the Beckwith-Bushnell model and (iii) less coding (and therefore less computer core storage) is required with the Van Driest-Clauser model than with the Beckwith-Bushnell model.

Each eddy viscosity model includes the Van Driest damping function in the "Law of the Wall" region. This function is semi-empirical and it is permissible to use either local or wall values of density and viscosity in the damping function. In previous finite-difference methods, little attention has been given to the effects of the choice of local or wall properties in the "Law of the Wall" region. In the present work, calculations have been made using both local and wall properties in the Van Driest damping function. For the Cary experimental conditions, the choice of properties in the damping function affected the predictions of skin-friction distributions by ten percent, but the effect was much smaller for the Kenworthy and Schetz experimental conditions. With the assumption of fully turbulent flow downstream of the slot, predictions with wall properties in the "Law of the Wall" region agreed better with the experimental data for the Cary conditions than did predictions with local properties. However, since experimental profile data for the Cary conditions were not available for comparison, a conclusive choice between local or wall properties in the Van Driest damping function cannot be made without further experimental data.

In the present finite-difference method, the energy and species conservation equations are for boundary-layer flows of two-component nonreacting gas mixtures, and slot injection of a foreign gas other than air could be considered; whereas, in the Beckwith and Bushnell finite-difference method, the energy and species conservation equations were specialized for air injection, and foreign gas injection could not be considered.

IX. REFERENCES

1. Davis, R. T., and Flugge-Lotz, I., "Second-Order Boundary Layer Effects in Hypersonic Flow Past Axisymmetric Blunt Bodies," J. Fluid Mechanics, Vol. 20, Part 4, 1964, pp. 593-623.

2. Davis, R. T., "The Hypersonic Fully Viscous Shock-Layer Problem," Sandia Laboratories Report SC-RR-68-840, Dec. 1968.

3. Davis, R. T., "Solution of the Viscous Shock-Layer Equations for a Binary Mixture," Nonreacting and Chemically Reacting Viscous Flows Over a Hyperboloid at Hypersonic Condition. Lewis, C. H., ed., AGARDograph No. 147, NATA, Paris, Sept. 1970, pp. 55-67.

4. Blottner, F. G., and Lenard, M., "Finite Rate Plasma Generation in the Laminar Air Boundary Layer of Slender Reentry Bodies," Transactions of the Eighth Symposium on Ballistic Missile and Space Technology, San Diego, California, 16-18 Oct. 1963, pp. 3-33.

5. Blottner, F. G., "Non-Equilibrium Laminar Boundary Layer Flow of Ionized Air," General Electric Report R64SD56. Also AIAA Journal, Vol. 2, No. 11, Nov. 1964, pp. 1921-1927.

6. Blottner, F. G., "Finite Difference Solution of the First-Order Boundary Layer Equations," Nonreacting and Chemically Reacting Viscous Flows Over a Hyperboloid at Hypersonic Condition. Lewis, C. H., ed., AGARDograph No. 147, NATO, Paris, Sept. 1970, pp. 13-36.

7. Crank, J., and Nicolson, P., "A Practical Method for Numerical Evaluation of Solutions of Partial Differential Equations of the Heat Conduction Type," Proc. Camb. Phil. Soc. Vol. 43, 1947, p. 50.

8. Patankar, S. V., and Spalding, D. B., Heat and Mass Transfer in Boundary Layers, C. R. C. Press, 1967.

9. Herring, H. James, and Mellor, George L., "A Method of Calculating Compressible Turbulent Boundary Layers," NASA CR-1144, 1968.

10. Cebeci, T., and Smith, A. M. O., "A Finite-Difference Solution of the Incompressible Turbulent Boundary-Layer Equations by an Eddy-Viscosity Concept," Douglas Aircraft Co., Report No. DAC-67130, Oct. 1968.

11. Cebeci, T., Smith, A. M. O., and Mosinskis, G., "Calculation of Compressible Adiabatic Turbulent Boundary Layers," AIAA Journal, Vol. 8, No. 11, Nov. 1970, pp. 1974-1982.

12. Elliott, D. G., Bartz, D. R., and Silver, S., "Calculation of Turbulent Boundary Layer Growth and Heat Transfer in Axisymmetric Nozzles," JPL TR-32-387, 1963.

13. Boldman, D. R., Newmann, H. E., and Schmidt, J. F., "Heat Transfer in 30° and 60° Half-Angle of Convergence Nozzles with Various Diameter Uncooled Pipe Inlets," NASA TN D-4177, 1967.

14. Pletcher, R. H., "On a Calculation Method for Compressible Turbulent Boundary Layer Flows with Heat Transfer," AIAA Paper 71-165, Jan. 1971.

15. Harris, J. E., "Numerical Solution of the Compressible Laminar, Transitional, and Turbulent Boundary Layer Equations," PhD Dissertation, VPI & SU, Blacksburg, Virginia, 1970.

16. Bushnell, Dennis M., Beckwith, Ivan E., "Calculation of Nonequilibrium Hypersonic Turbulent Boundary Layers and Comparisons with Experimental Data," AIAA Journal, Vol. 8, No. 8, Aug. 1970, pp. 1462-1469.

17. Anderson, E. C., and Lewis, C. H., "Laminar or Turbulent Boundary-Layer Flows of Perfect Gases or Reacting Gas Mixtures in Chemical Equilibrium," NASA CR-1893, 1971.

18. Lewis, C. H., Anderson, E. C., and Miner, E. W., "Nonreacting and Equilibrium Chemically Reacting Turbulent Boundary-Layer Flows," AIAA Paper No. 71-597, June 1971.

19. Lewis, C. H., Miner, E. W., and Anderson, E. C., "Effects of Strong Axial Pressure Gradients on Turbulent Boundary-Layer Flows," Paper No. 21, in AGARD-CP-93, London, September 1971.

20. Miner, E. W., Anderson, E. C., and Lewis, C. H., "A Computer Program for Two-Dimensional and Axisymmetric Nonreacting Perfect Gas and Equiilibrium Chemically Reacting Laminar, Transitional and/or Turbulent Boundary-Layer Flows," College of Engineering Report VPI-E-71-8, VPI & SU, Blacksburg, Virginia, May 1971.

21. Cary, Aubrey M., Jr., and Hefner, Jerry N., "Film Cooling Effectiveness in Hypersonic Turbulent Flow," AIAA Journal, Vol. 8, No. 11, Nov. 1970, pp. 2090-2091.

22. Bushnell, Dennis M., "Calculation of Relaxing Turbulent Boundary Layers Downstream of Tangential Slot Injection," J. Spacecraft, Vol. 8, No. 5, May 1971, pp. 550-551.

23. Beckwith, I. E., and Bushnell, D. M., "Calculation by a Finite-Difference Method of Supersonic Turbulent Boundary Layers with Tangential Slot Injection," NASA TN D-6221, 1971.

24. Cary, A. M., Jr., and Hefner, J. N., "An Investigation of Film-Cooling Effectiveness and Skin Friction in Hypersonic Turbulent Flow," AIAA Paper No. 71-599, June 1971.

25. Kurkov, Anatole P., "Mixing of Supersonic Jets Including the Effects of Transverse Pressure Gradient Using Difference Methods," NASA TN D-6593, 1971.

26. Van Dyke, M., "Second-Order Compressible Boundary-Layer Theory with Application to Blunt Bodies in Hypersonic Flow," Stanford University Report SUDAER No. 112, 1961.

27. Jaffe, N. A., Lind, R. C., and Smith, A. M. O., "Solution to the Binary Diffusion Laminar Boundary Layer Equations Including the Effect of Second-Order Transverse Curvature," Report LB32613, January 1966, Douglas Aircraft Company.

28. Van Driest, E. R., "On Turbulent Flow Near a Wall," J. Aero. Sci., Vol. 23, No. 11, Nov. 1956, pp. 1008-1011, 1036.

29. Bushnell, D. M., Morris, D. J., "Eddy Viscosity Distributions in a Mach 20 Turbulent Boundary Layer," AIAA Journal, Vol. 9, No. 4, April 1971, pp. 764-766.

30. Kenworthy, M. A., and Schetz, J. A., "An Experimental Study of Slot Injection into a Supersonic Stream," NASA, Contractor Report to be published.

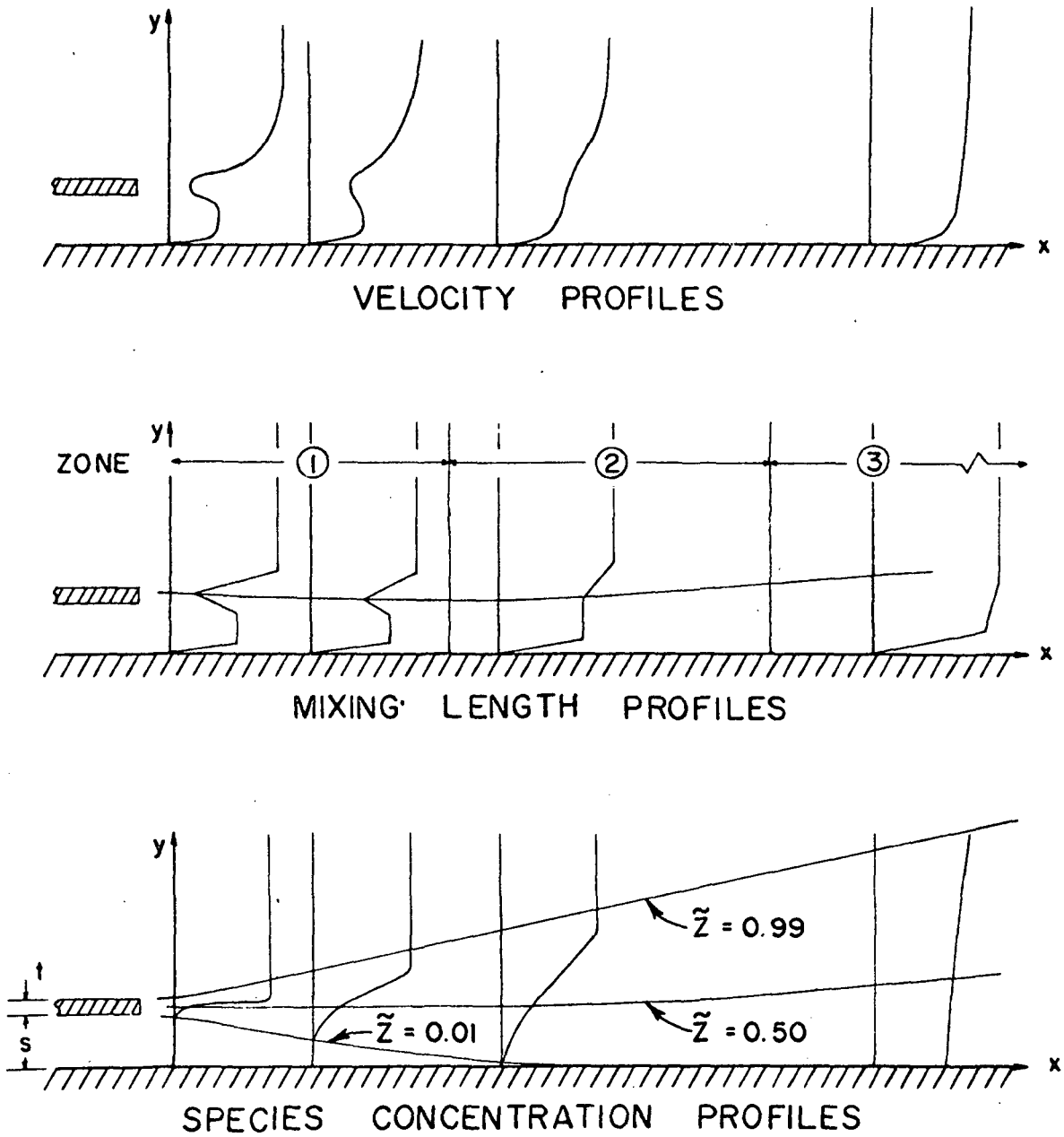

Figure 1: Schematic of Slot Injection Flow Field

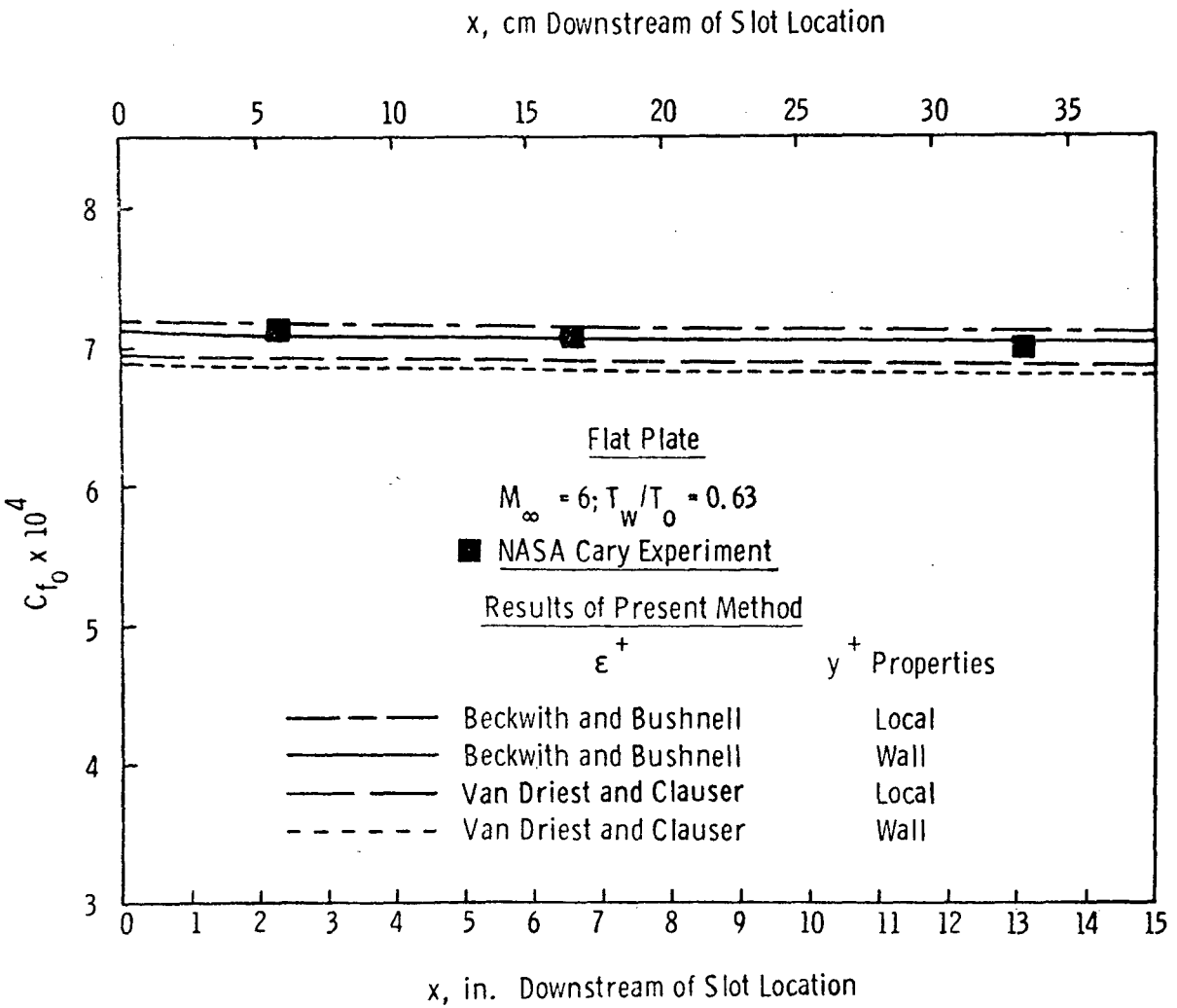

Figure 2: Skin-Friction Distributions for Flat Plate Flow, NASA Cary Conditions

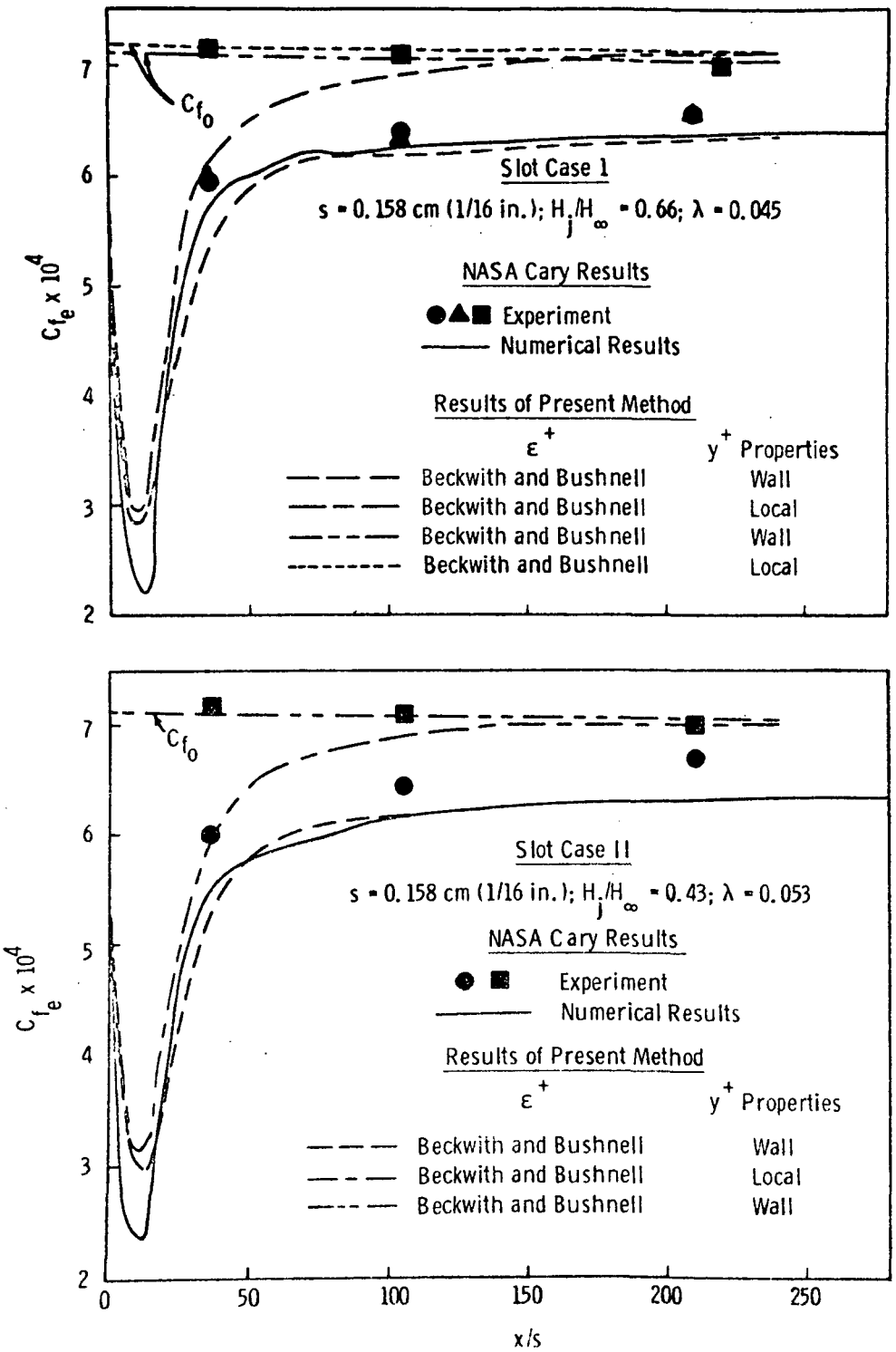

Figure 3: Skin-Friction Distributions with Slot Injection, NASA Cary Conditions

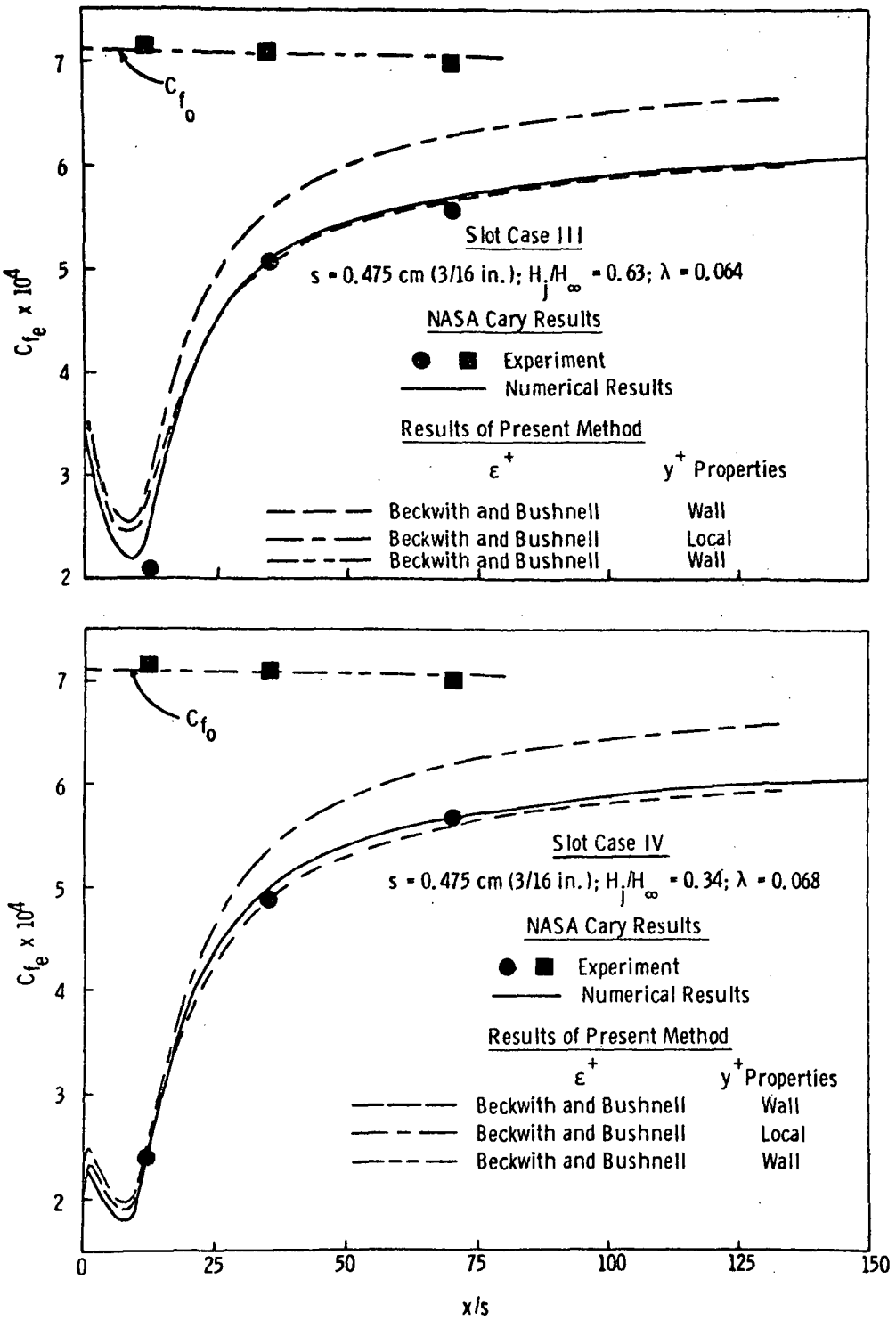

Figure 3: Continued

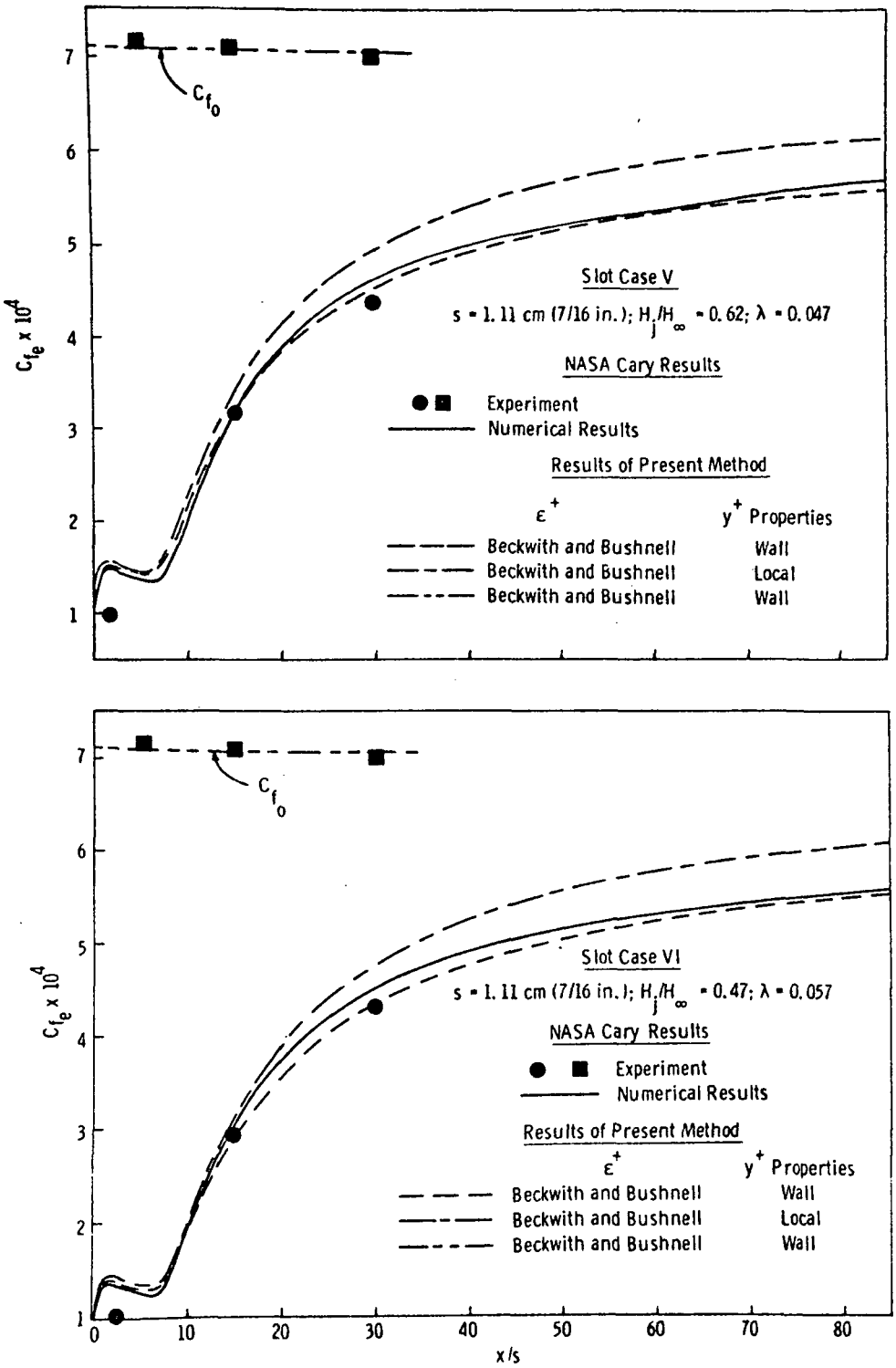

Figure 3: Concluded

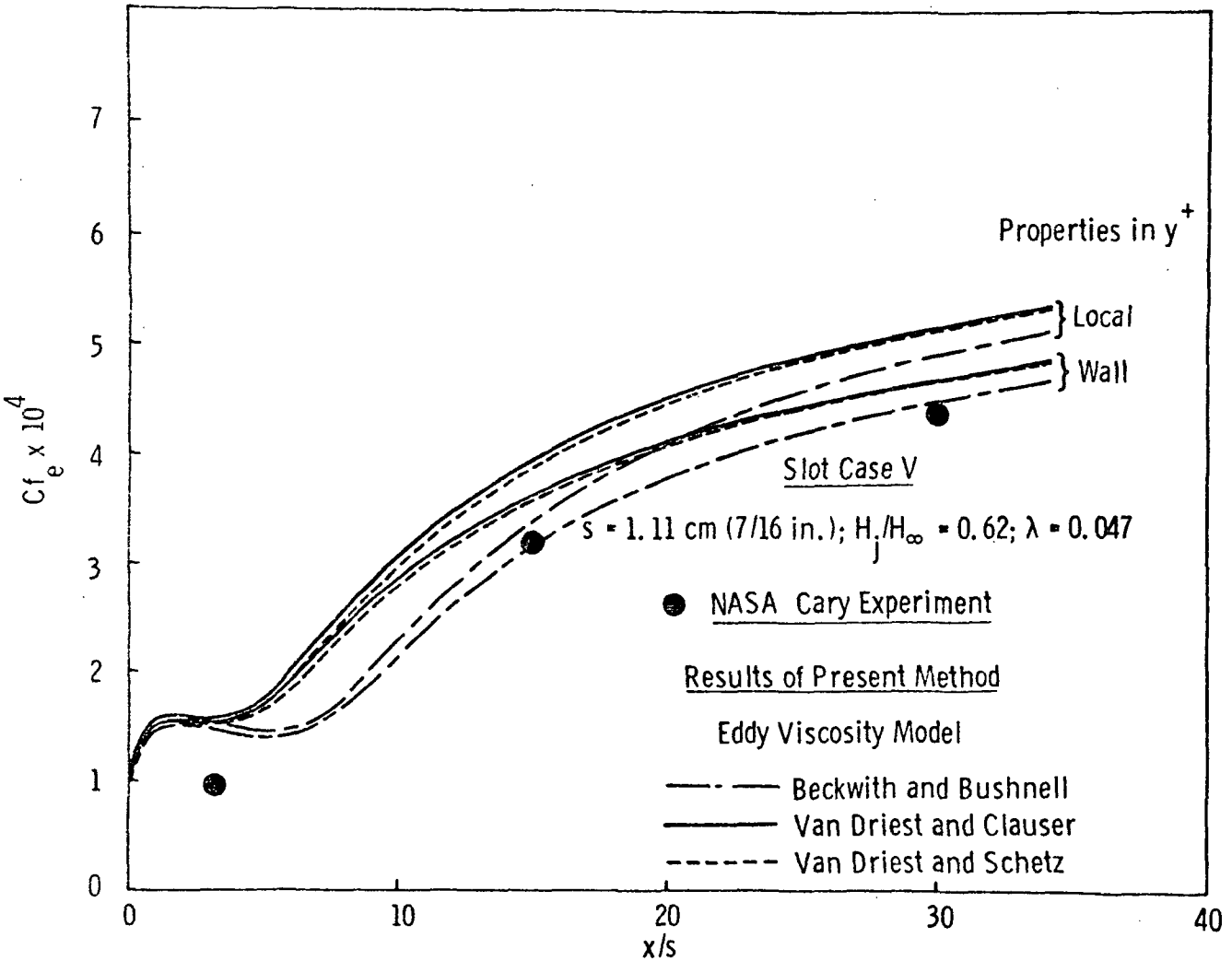

Figure 4: Comparison of Predicted Skin-Friction Distributions with Different Eddy Viscosity Models, NASA Cary Conditions, Case V

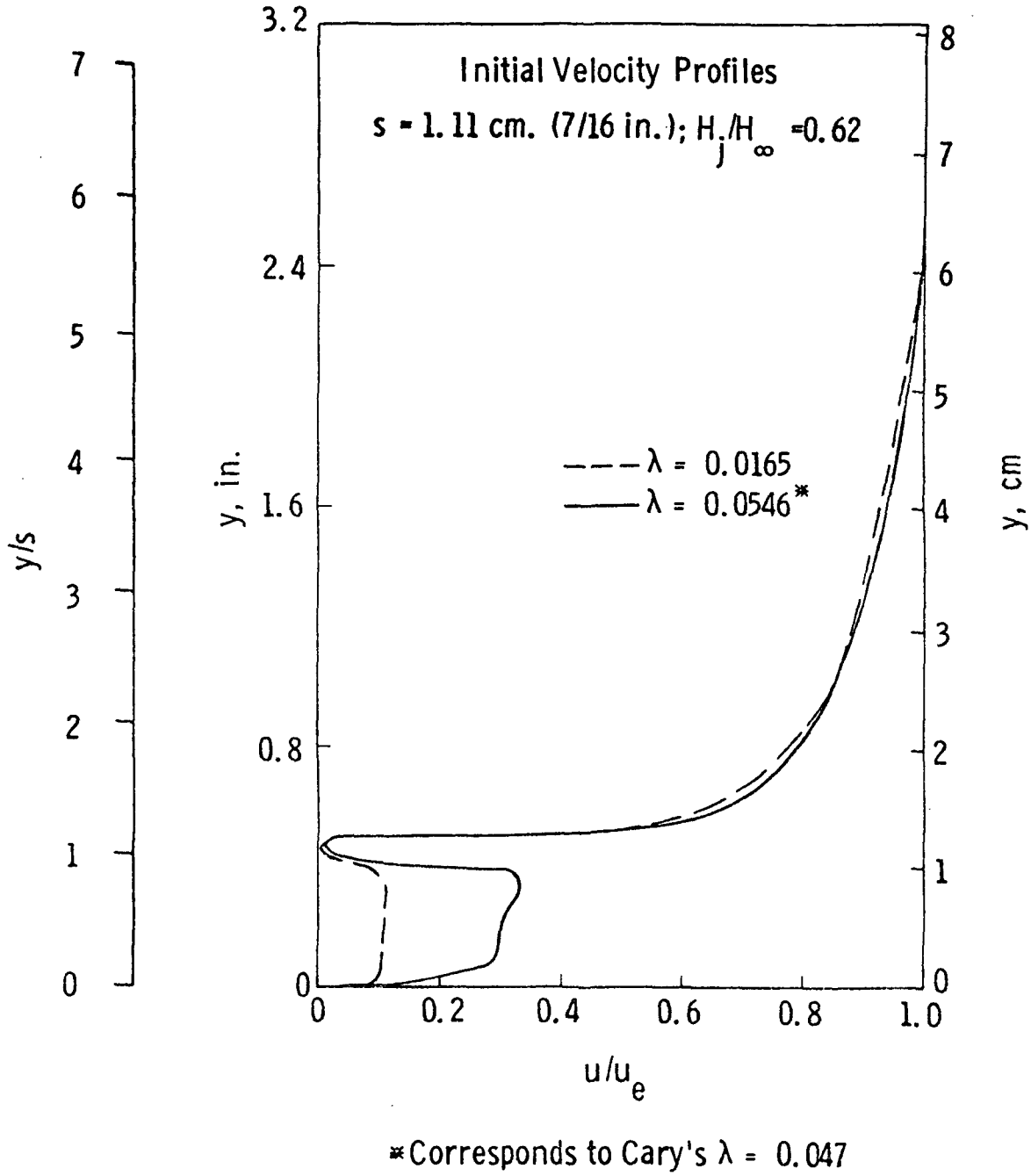

Figure 5: Initial Velocity Profiles for Slot Injection Calculations, NASA Cary Case V Conditions

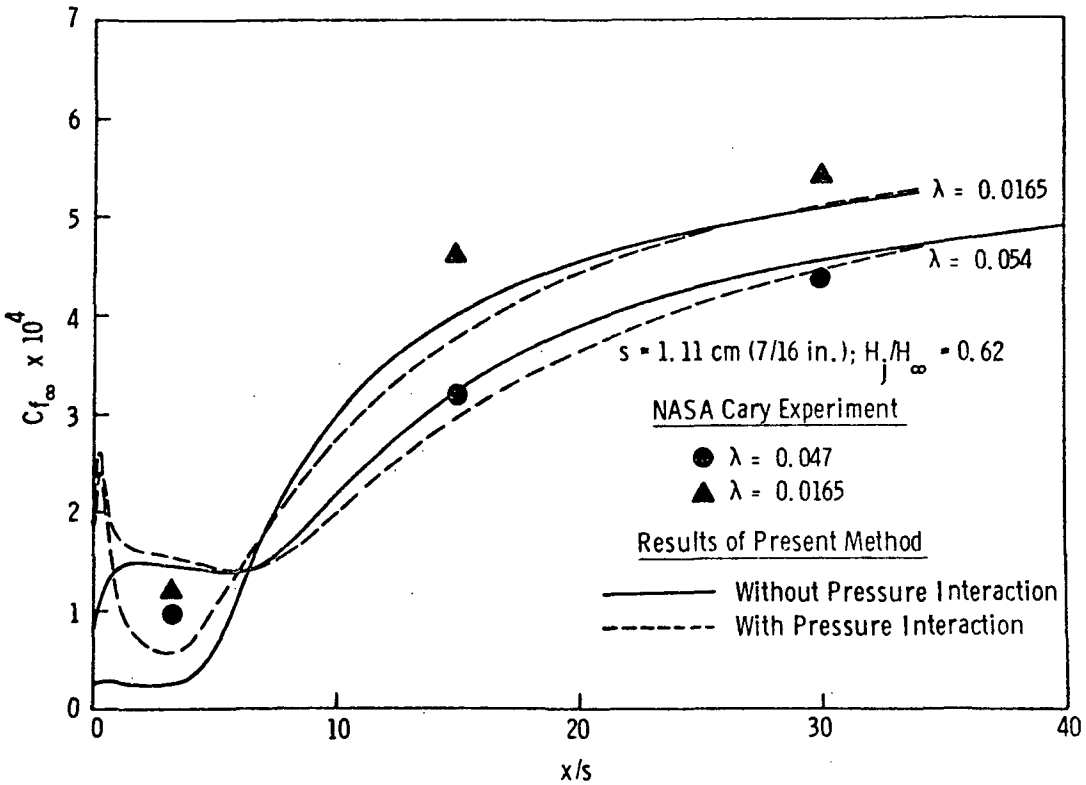

Figure 6: Predicted Skin-Friction Distributions with and without Pressure Interaction, NASA Cary Case V Conditions, with Beckwith-Bushnell ϵ^+

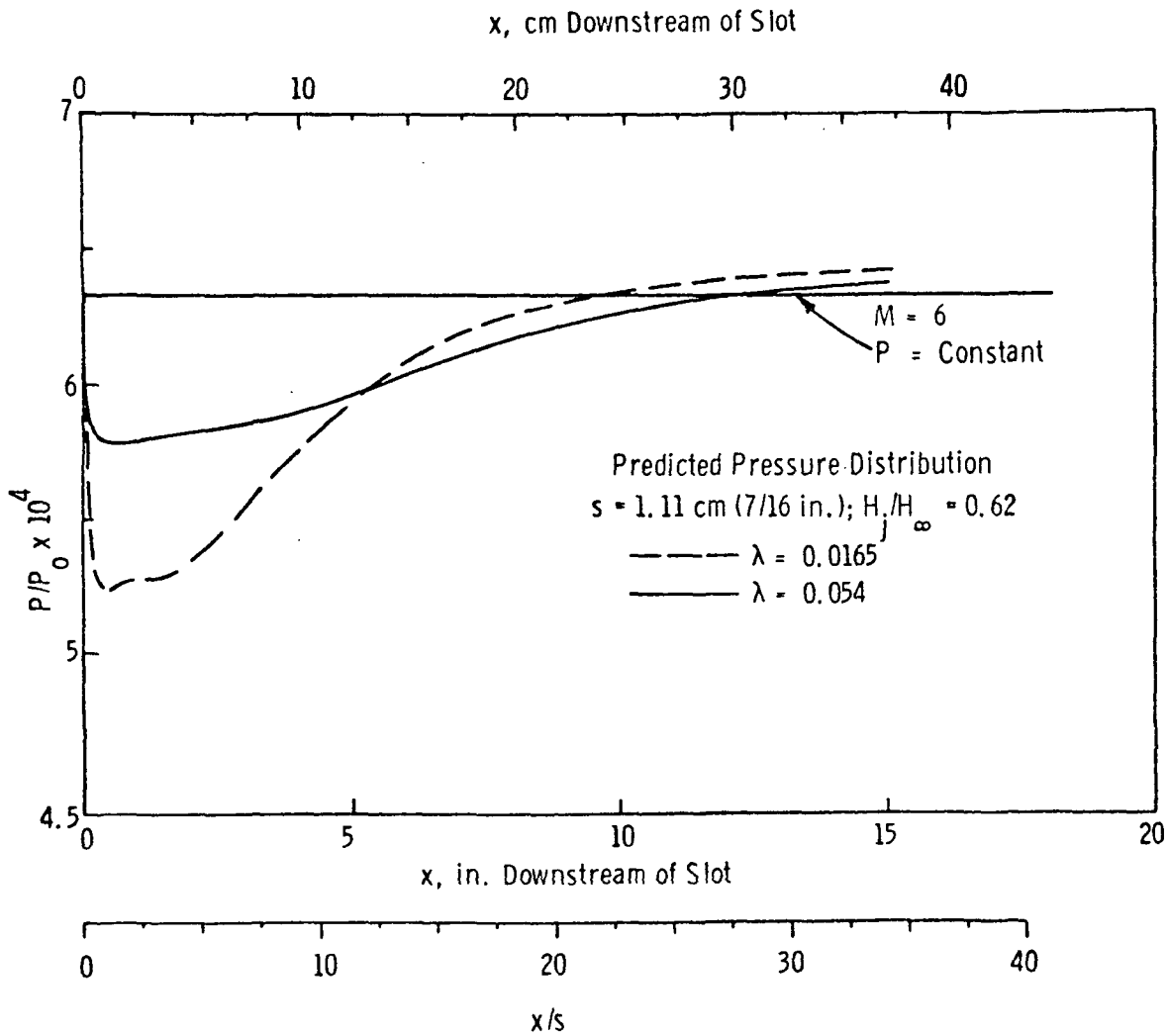

Figure 7: Predicted Wall Static Pressure Distributions with Pressure Interaction, NASA Cary Case V Conditions

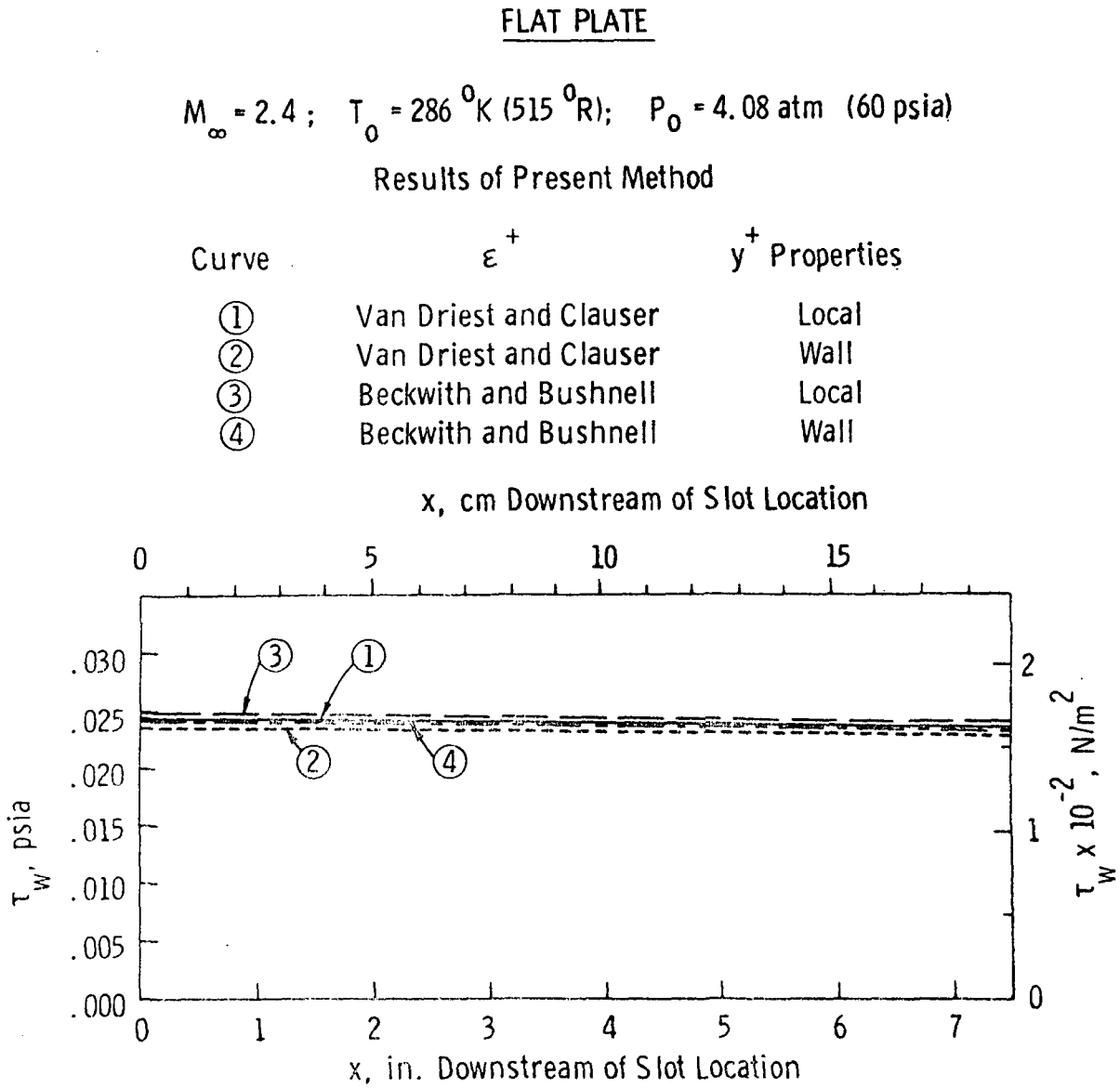

Figure 8: Predicted Wall Shear Stress Distributions for Flat Plate Flow, VPI Conditions

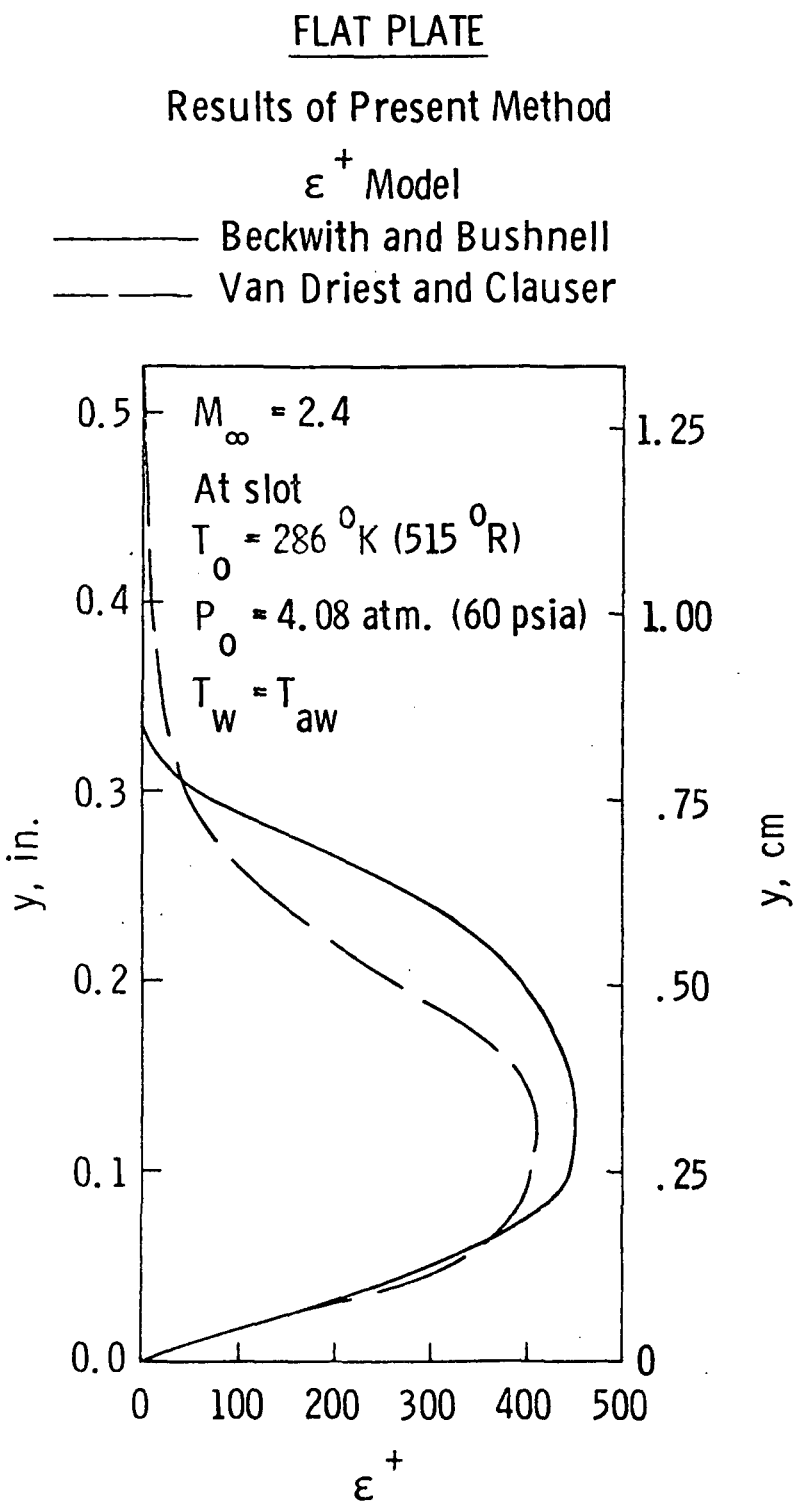

Figure 9: Comparison of Eddy Viscosity Profiles for Flat Plate Flow at Slot Location, VPI Conditions

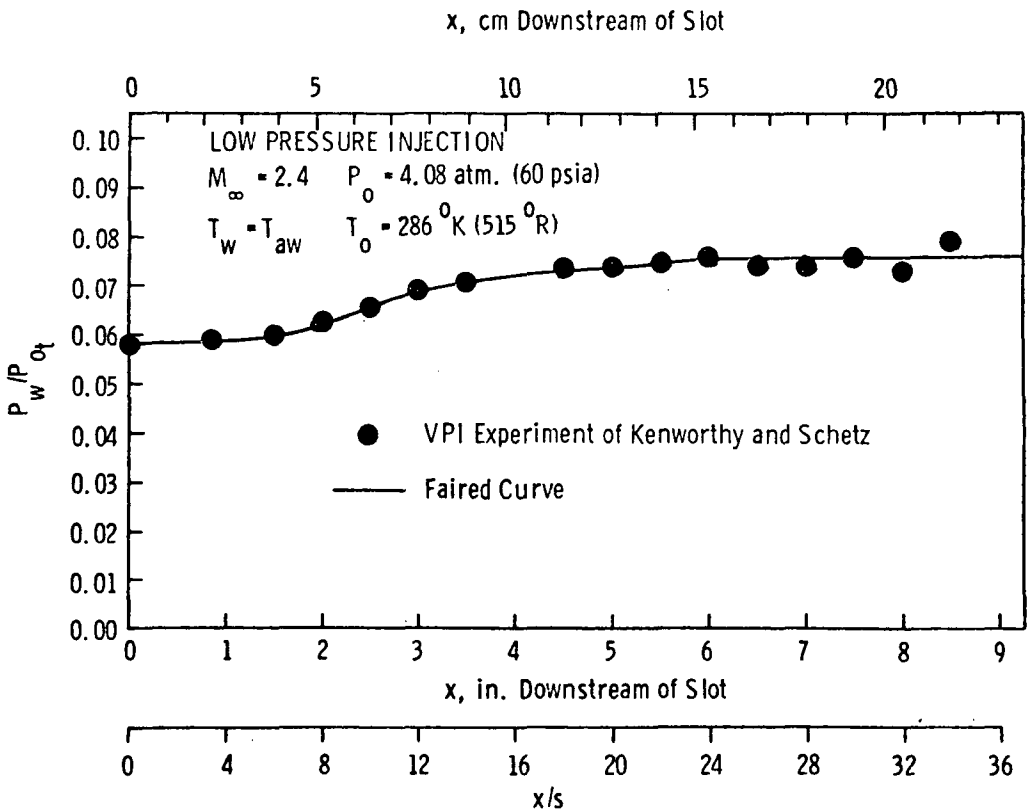

Figure 10: Wall Static Pressure Distributions for Low Pressure Injection, VPI Conditions

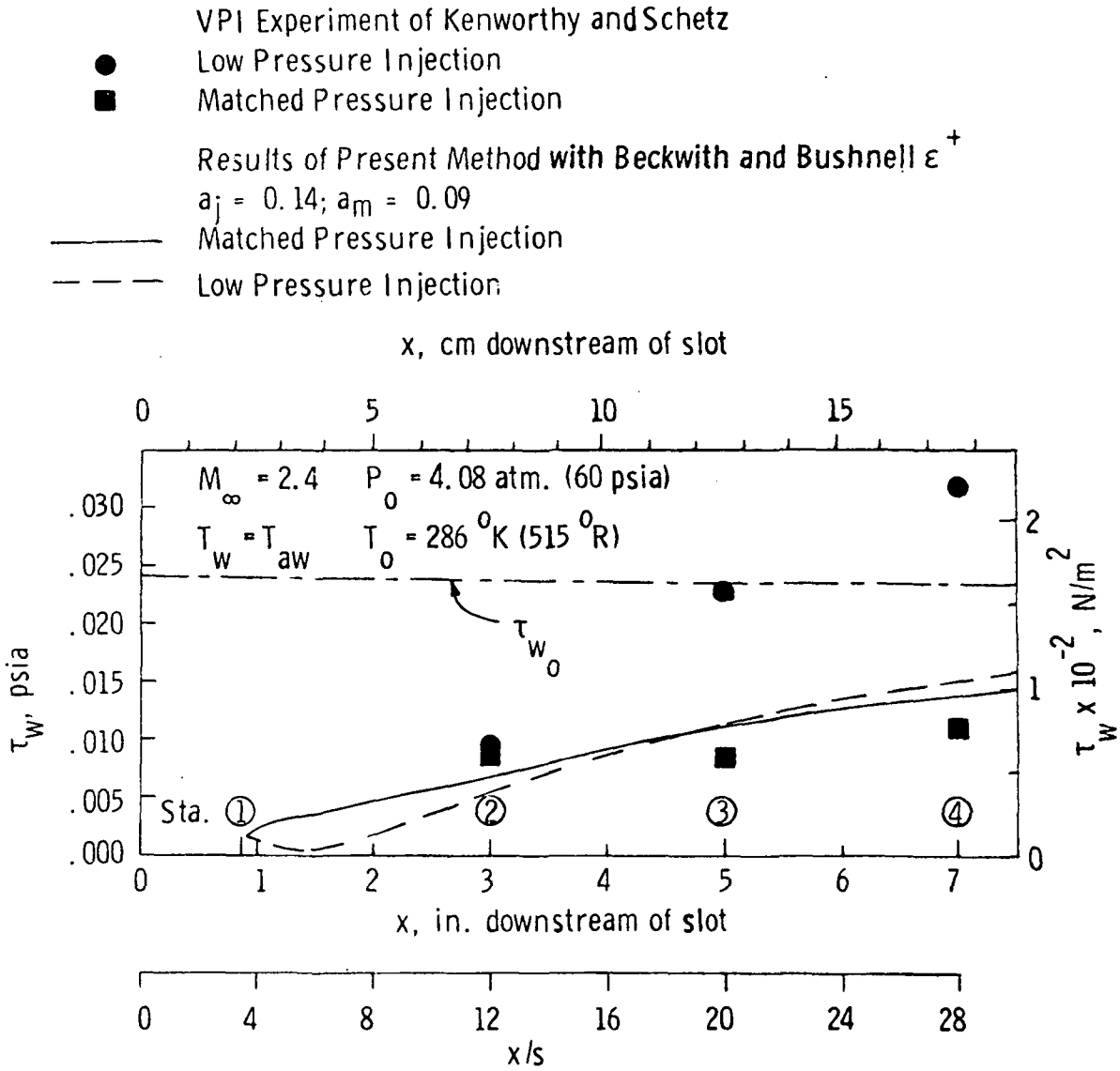

Figure 11: Comparison of Wall Shear Stress Distributions, VPI Conditions

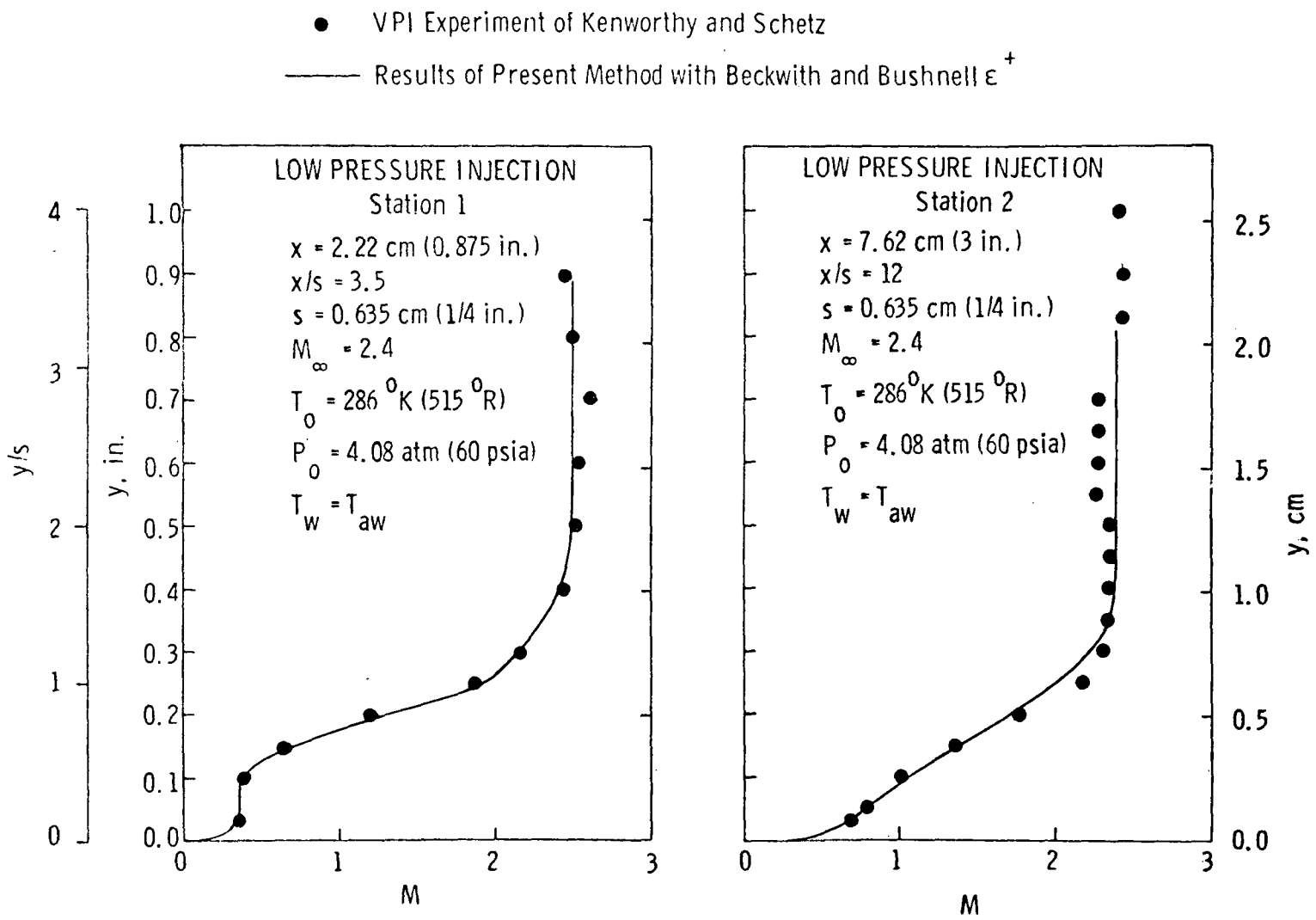

Figure 12: Comparison of Mach Number Profiles, Low Pressure Injection, VPI Conditions

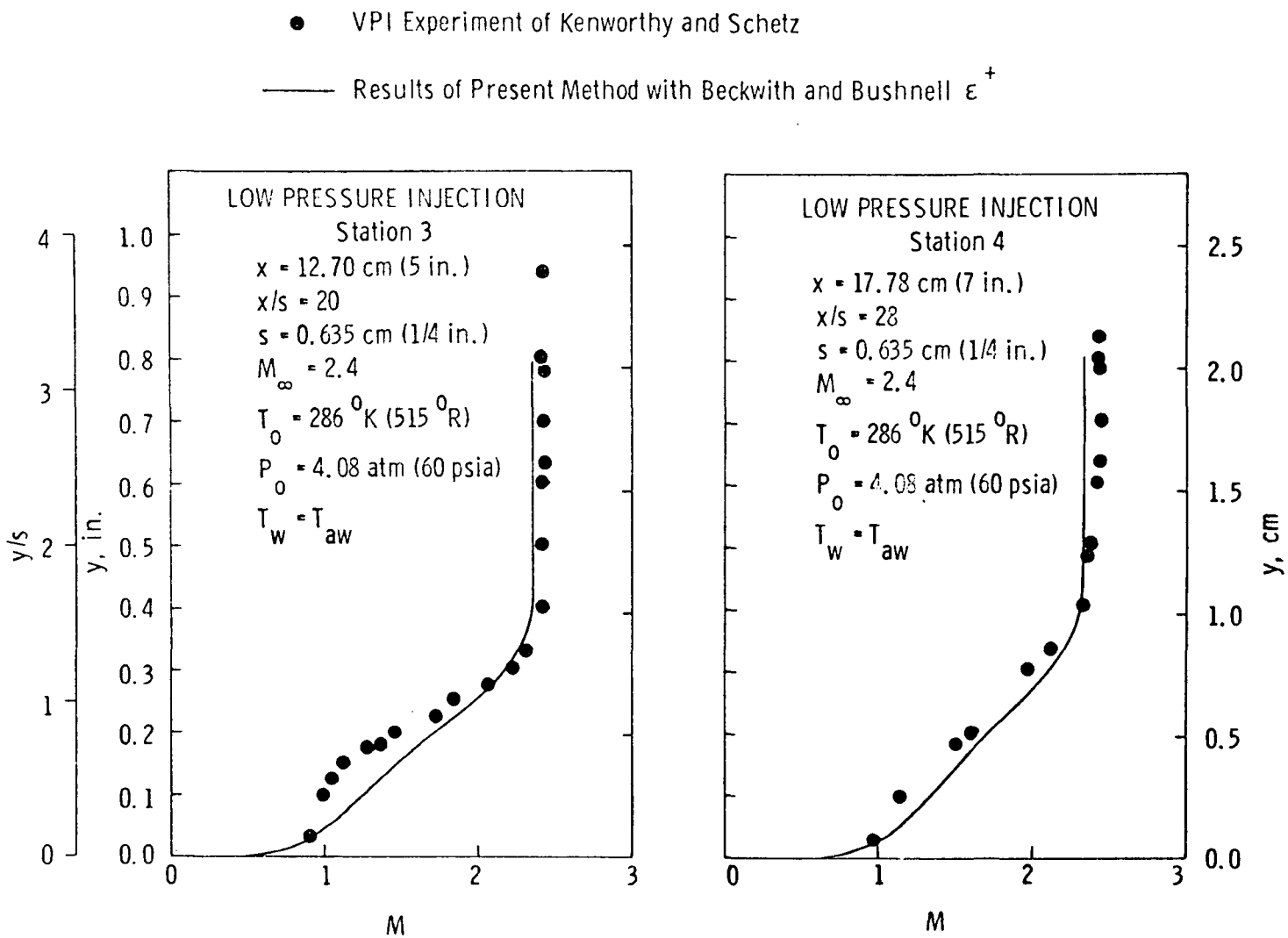

Figure 12: Concluded

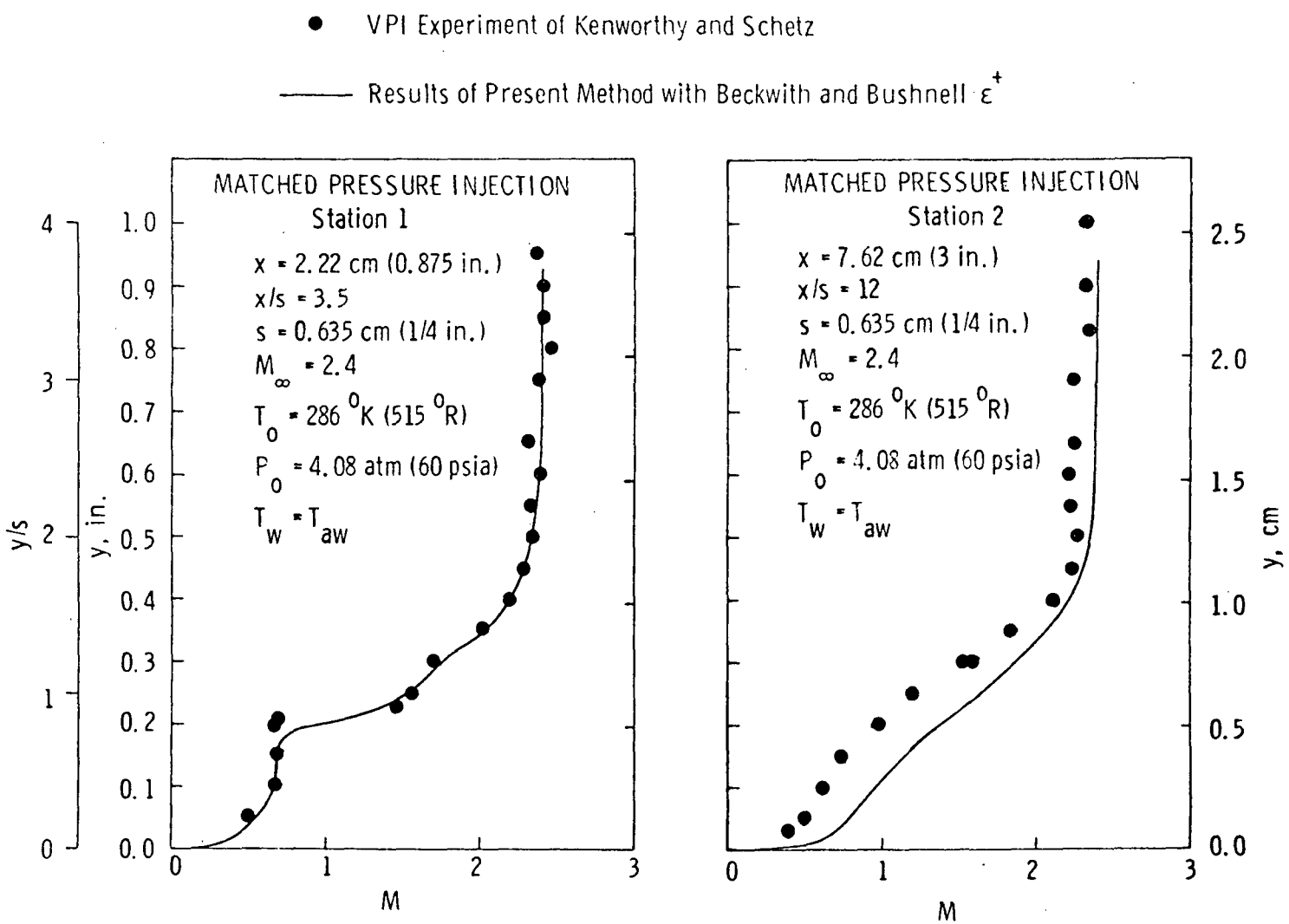

Figure 13: Comparison of Mach Number Profiles, Matched Pressure Injection, VPI Conditions

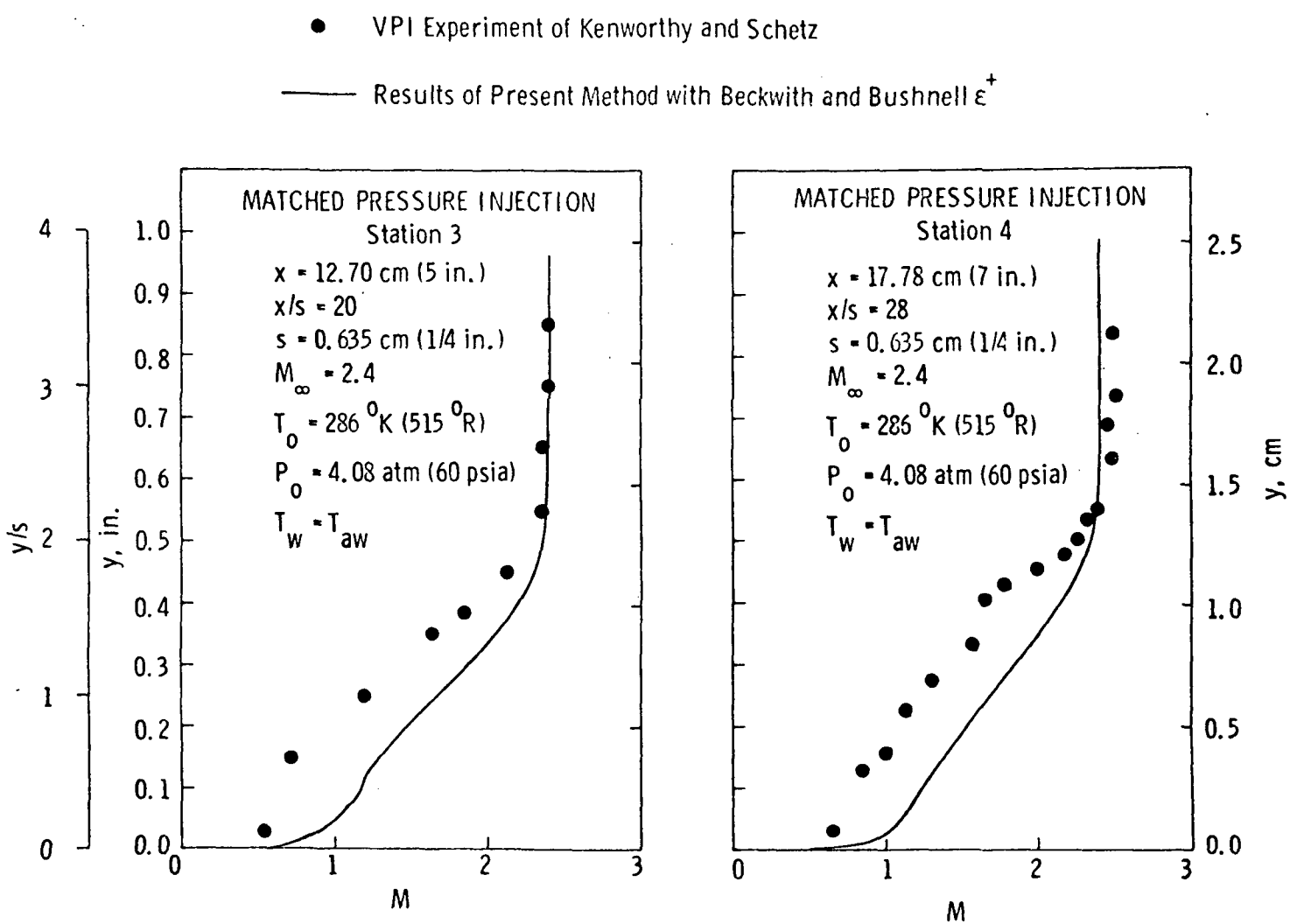

Figure 13: Concluded

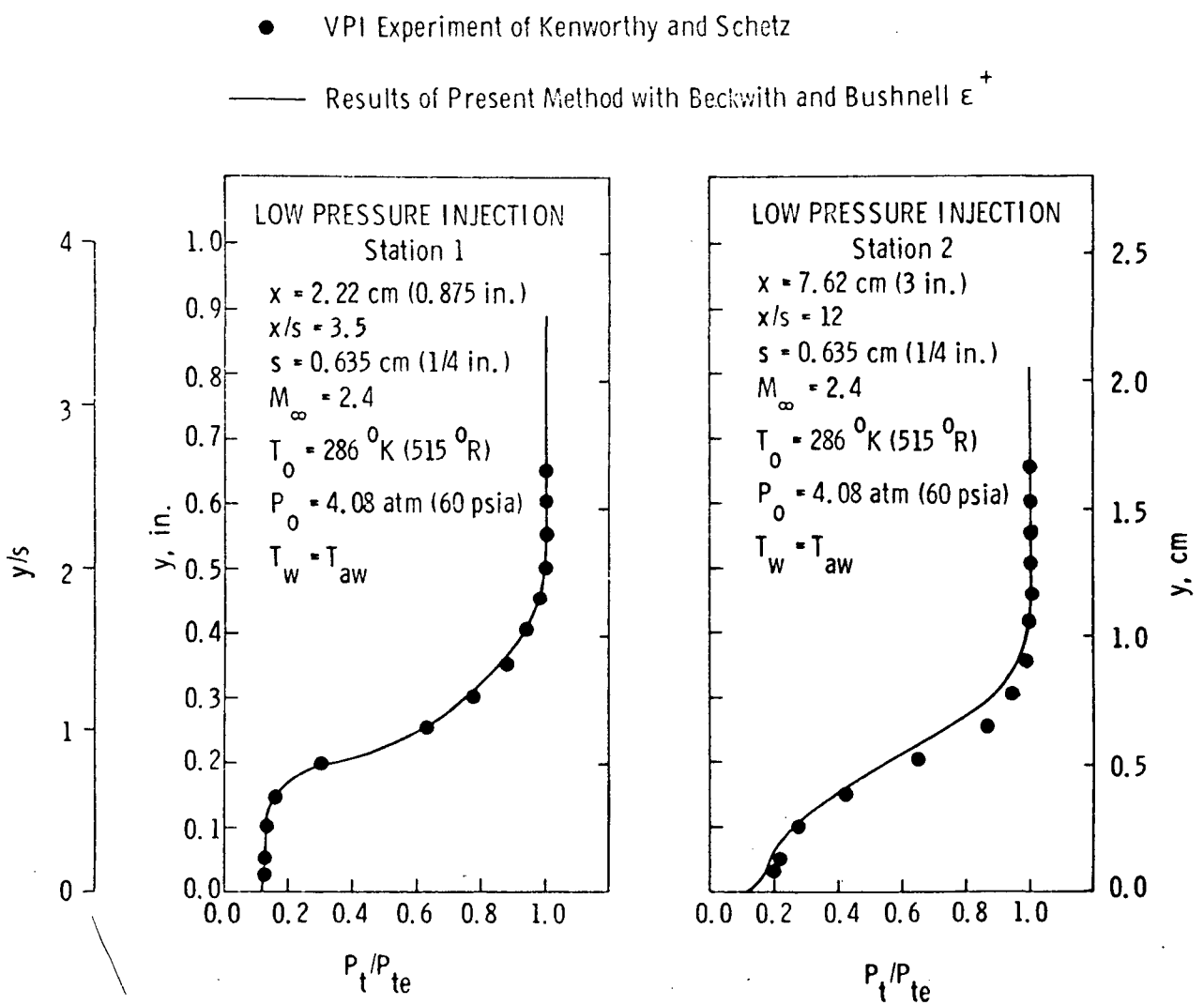

Figure 14: Comparison of Pitot Pressure Profiles, Low Pressure Injection, VPI Conditions

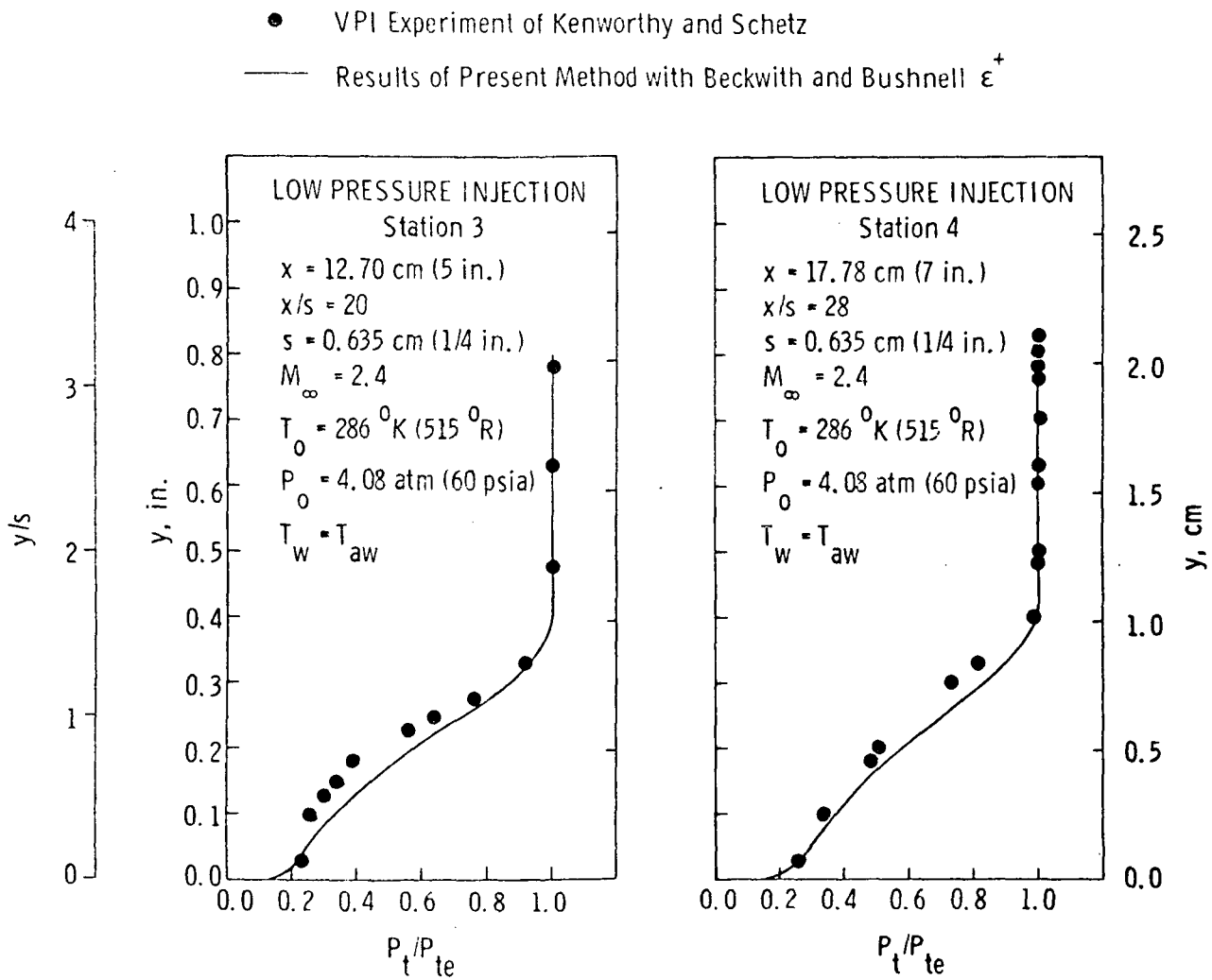

Figure 14: Concluded

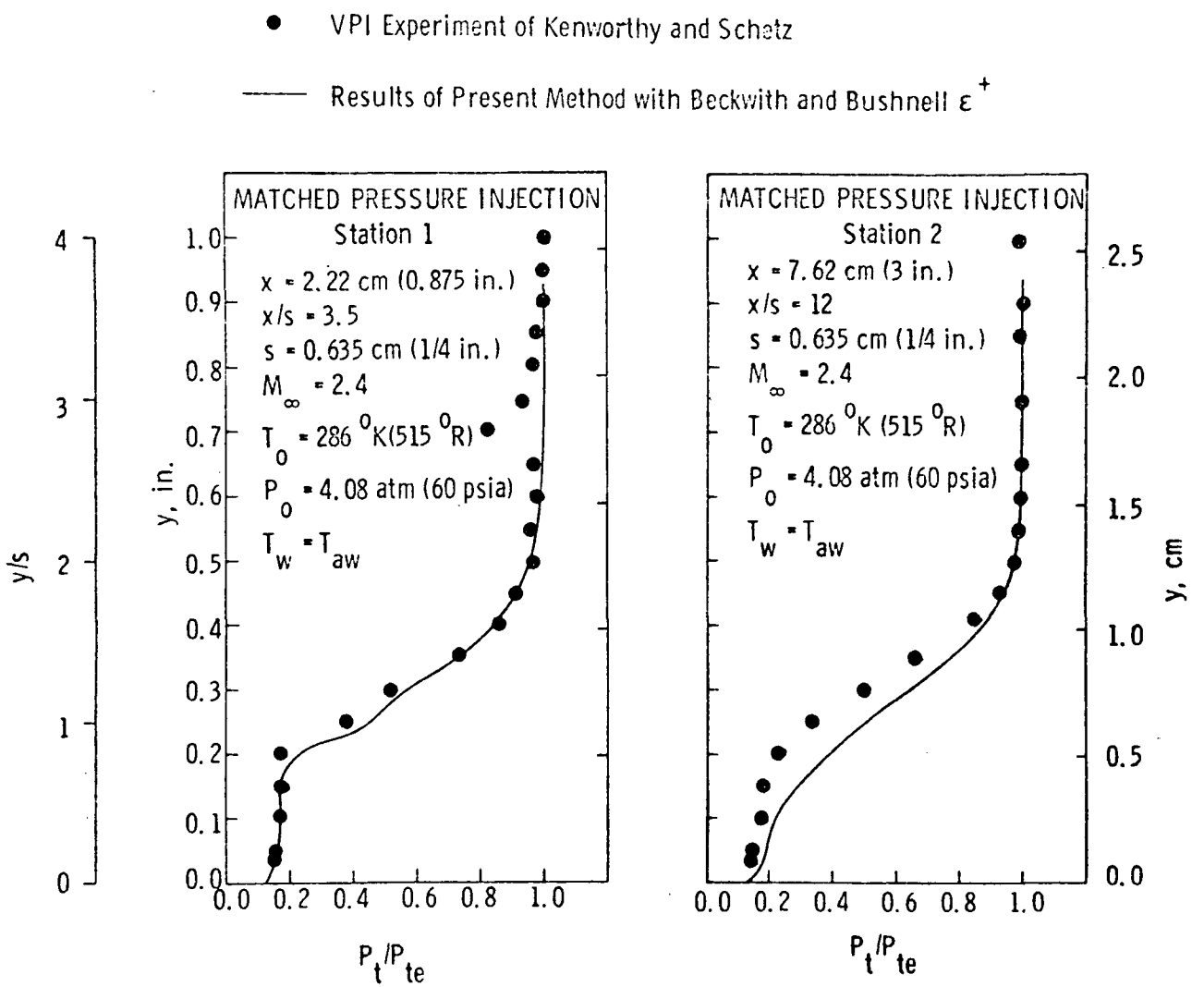

Figure 15: Comparison of Pitot Pressure Profiles, Matched Pressure Injection, VPI Conditions

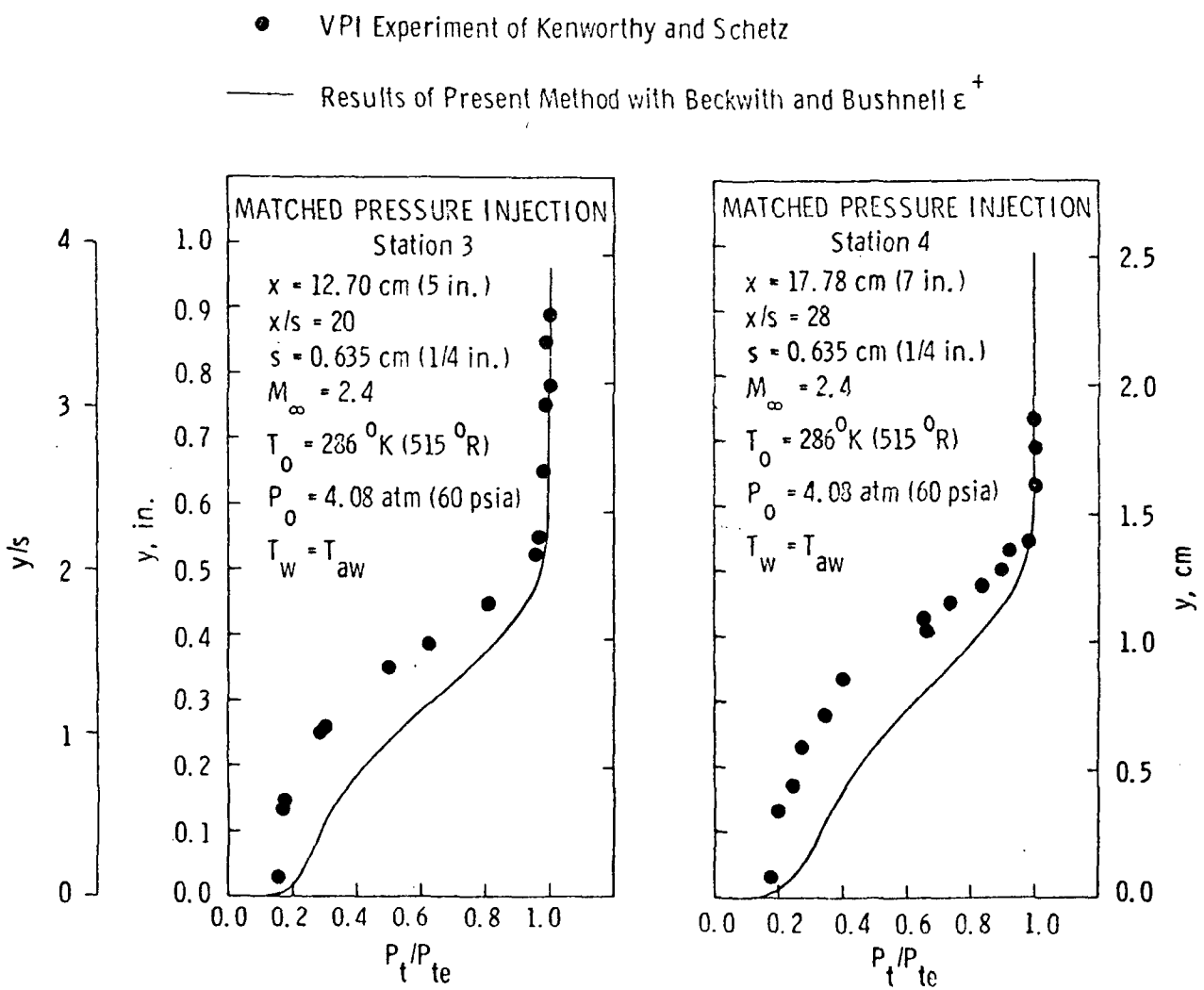

Figure 15: Concluded

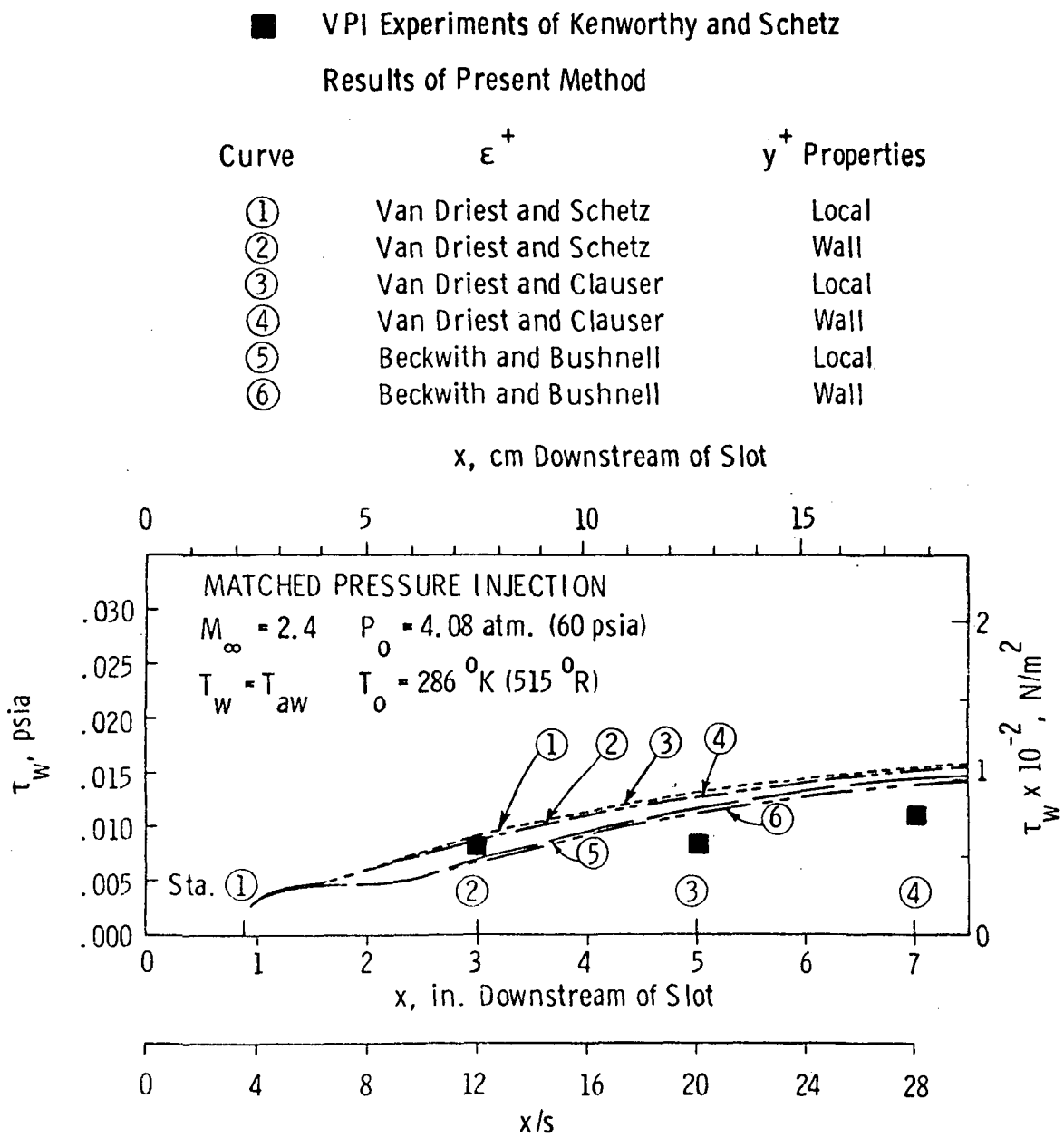

Figure 16: Comparison of Predicted Wall Shear Stress Distributions with Different Eddy Viscosity Models, VPI Conditions

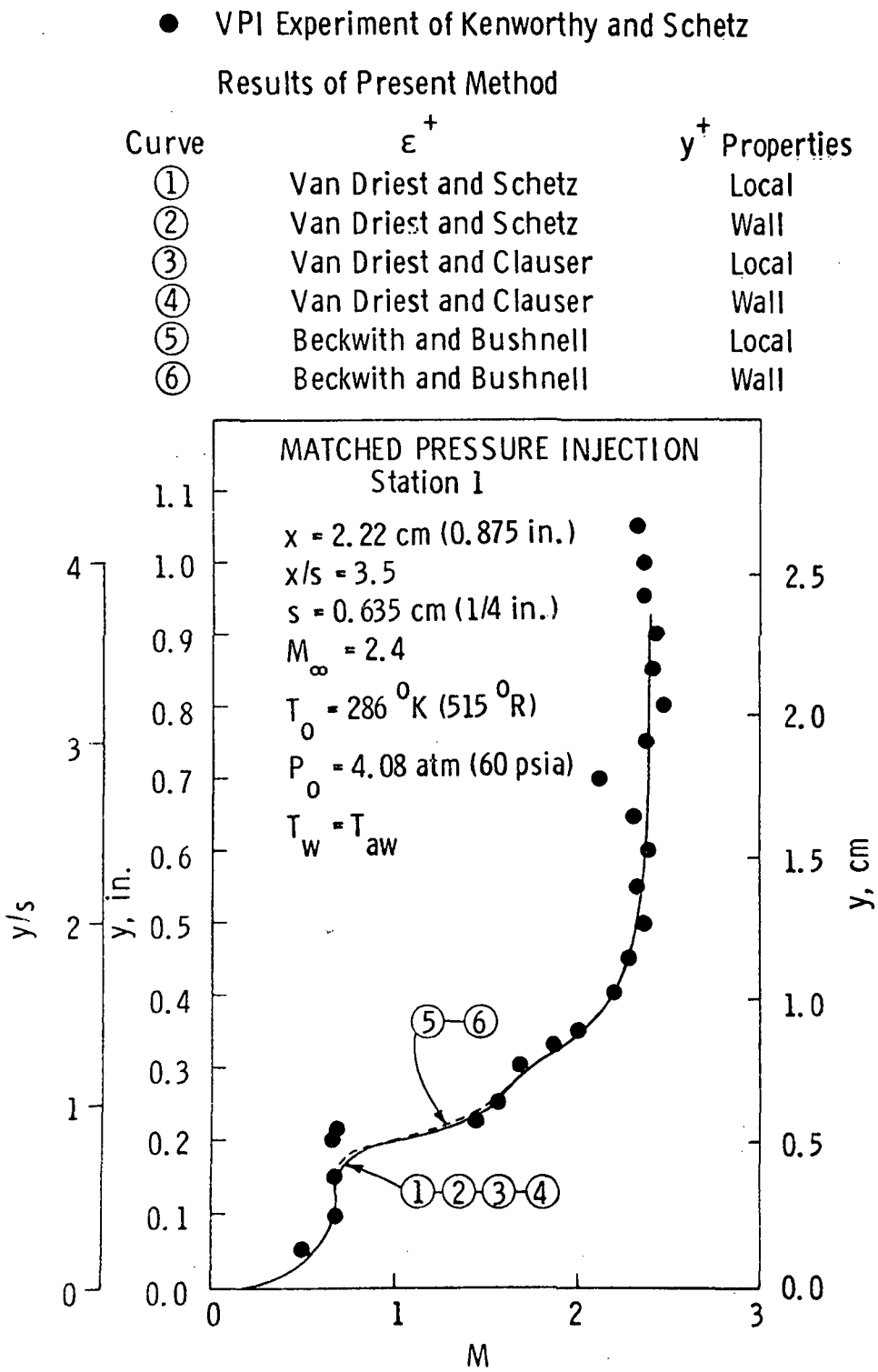

Figure 17: Comparison of Mach Number Profiles with Different Eddy Viscosity Models; Station 1, VPI Conditions

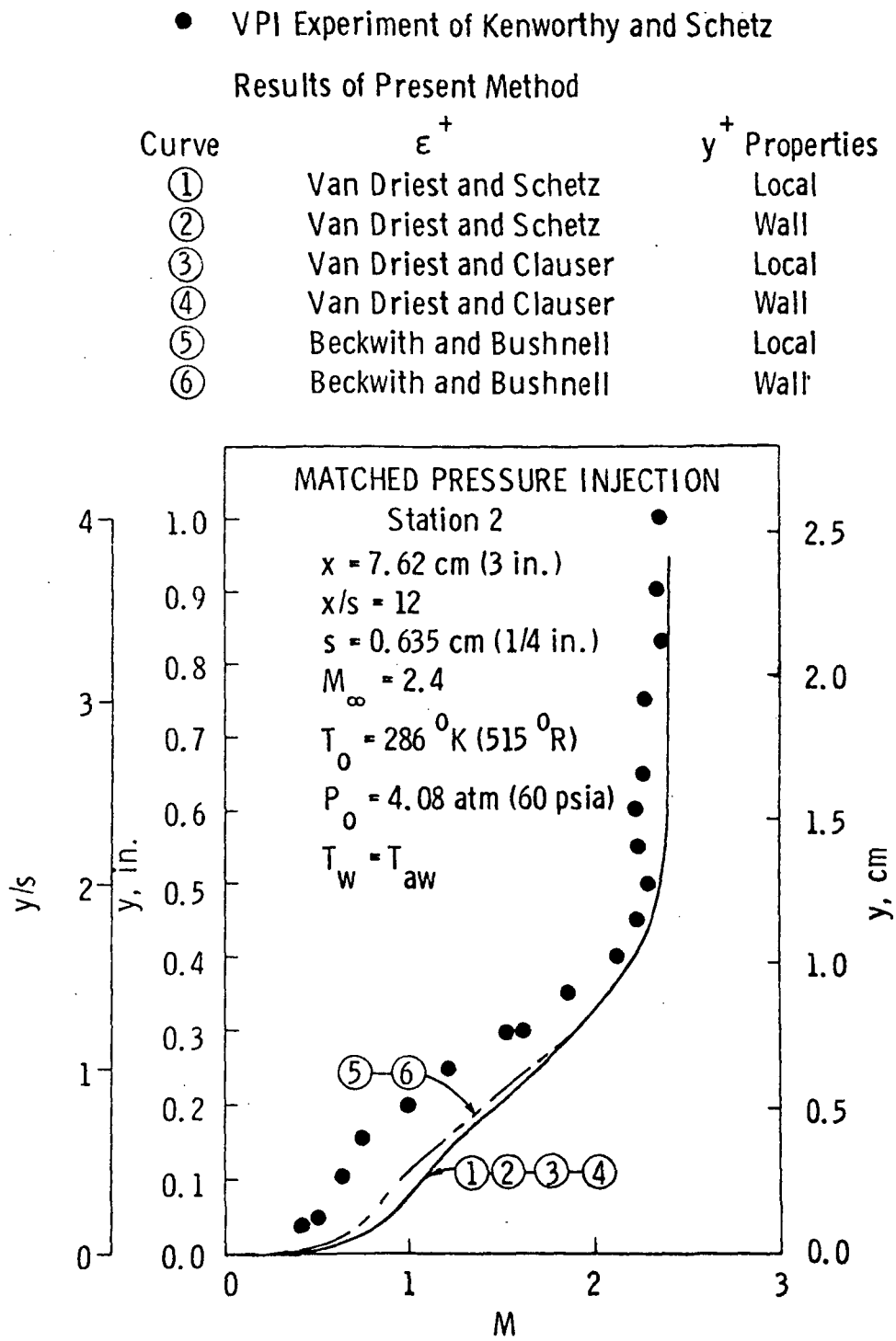

Figure 18: Comparison of Mach Number Profiles with Different Eddy Viscosity Models; Station 2, VPI Conditions

- VPI Experiment of Kenworthy and Schetz

Results of Present Method

Curve	ε^+	y^+ Properties
①	Van Driest and Schetz	Local
②	Van Driest and Schetz	Wall
③	Van Driest and Clauser	Local
④	Van Driest and Clauser	Wall
⑤	Beckwith and Bushnell	Local
⑥	Beckwith and Bushnell	Wall

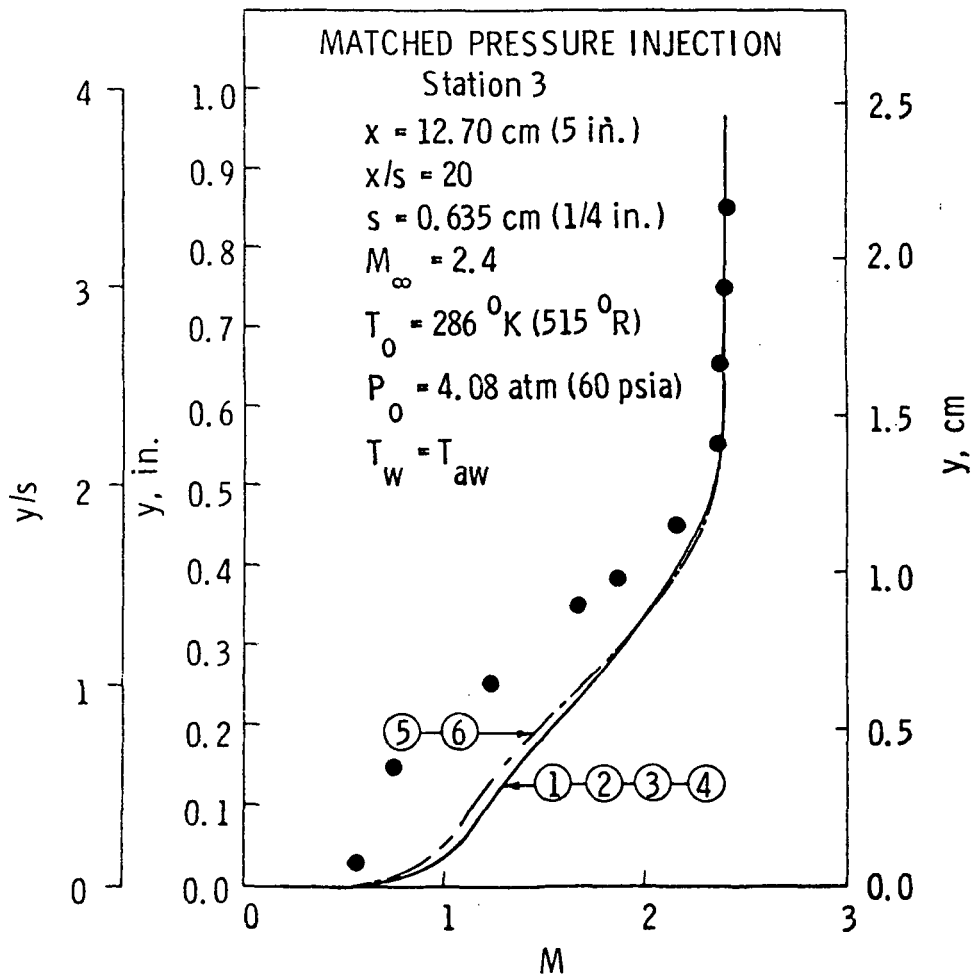

Figure 19: Comparison of Mach Number Profiles with Different Eddy Viscosity Models; Station 3, VPI Conditions

- VPI Experiment of Kenworthy and Schetz

Results of Present Method

Curve	ε^+	y^+ Properties
①	Van Driest and Schetz	Local
②	Van Driest and Schetz	Wall
③	Van Driest and Clauser	Local
④	Van Driest and Clauser	Wall
⑤	Beckwith and Bushnell	Local
⑥	Beckwith and Bushnell	Wall

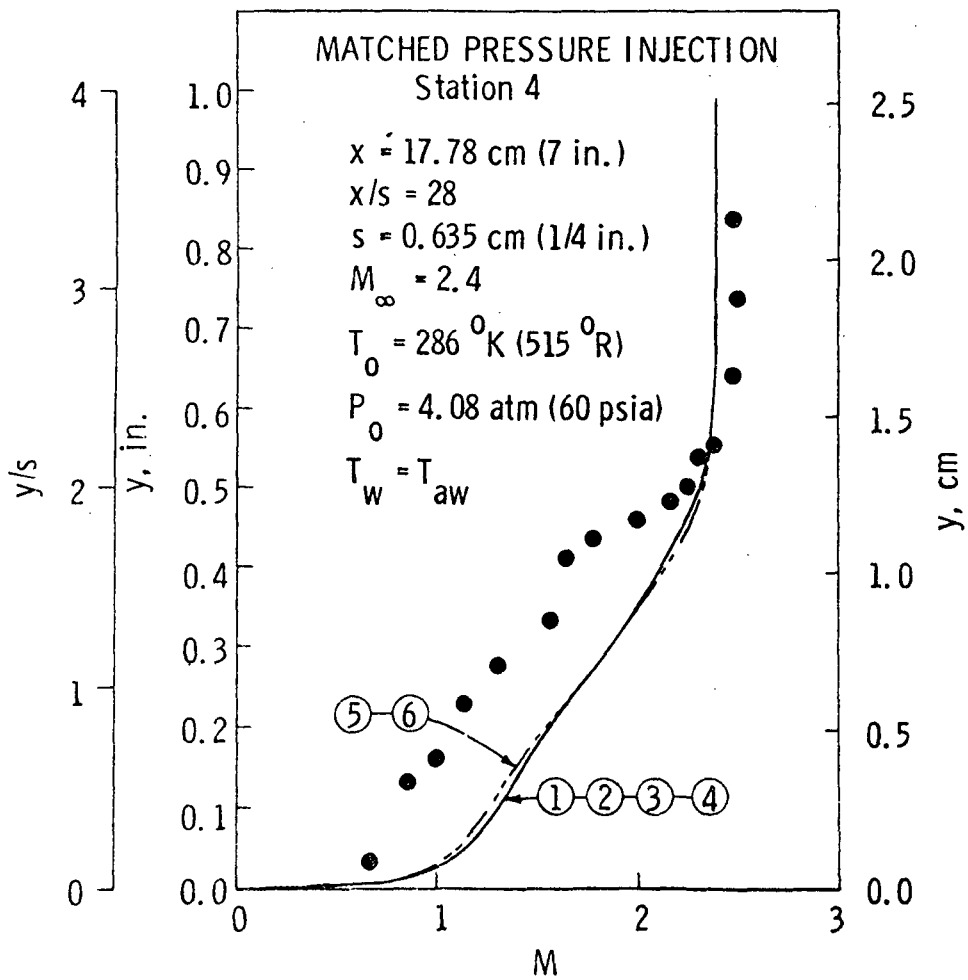

Figure 20: Comparison of Mach Number Profiles with Different Eddy Viscosity Models, Station 4, VPI Conditions

■ VPI Experiment of Kenworthy and Schetz

Results of Present Method with Beckwith and Bushnell ε^+

Curve	a_j	a_m	SLOT	MIXING
①	0.14	0.09	Turbulent	Turbulent
②	0.14	0.05	Turbulent	Turbulent
③	0.14	0.01	Turbulent	Laminar
④	0.014	0.09	Laminar	Turbulent
⑤	0.014	0.05	Laminar	Turbulent
⑥	0.014	0.01	Laminar	Laminar

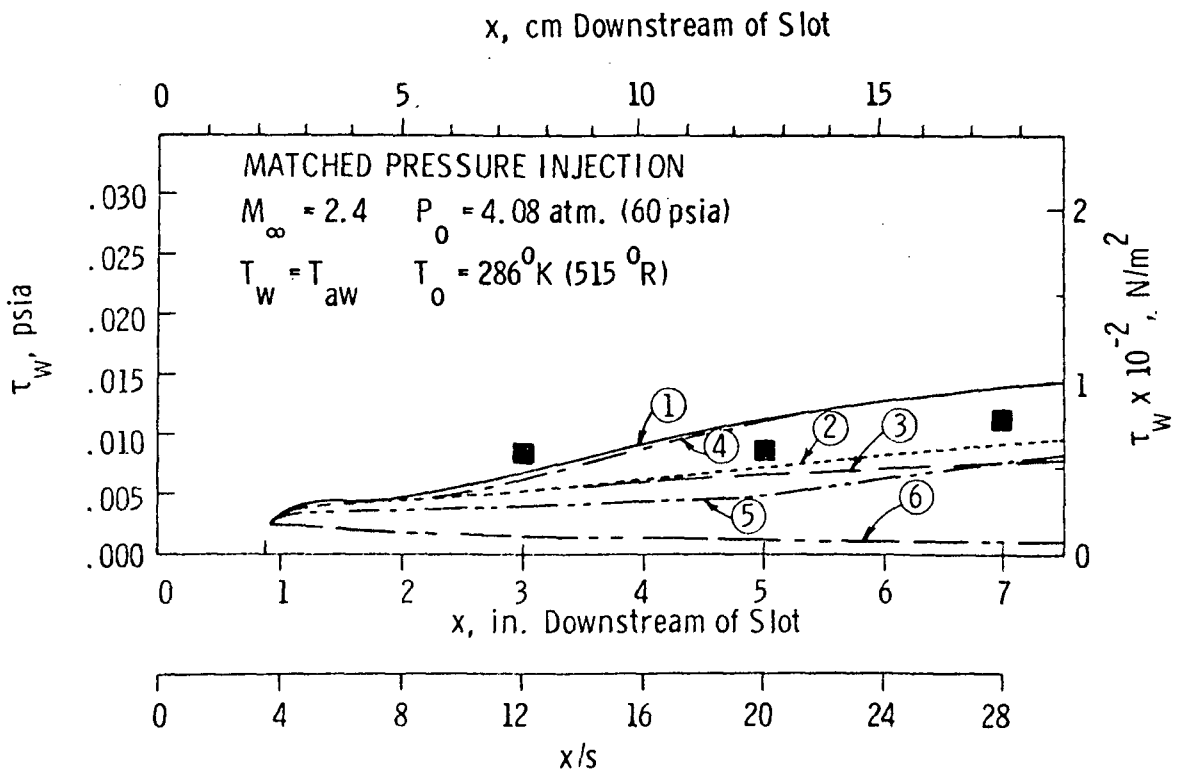

Figure 21: Comparison of Wall Shear Stress Distributions with Laminar and Turbulent Slot Flow and Mixing, VPI Conditions

- VPI Experiment of Kenworthy and Schetz

Results of Present Method with Beckwith and Bushnell ε^+

Curve	a_j	a_m	SLOT	MIXING
①	0.14	0.09	Turbulent	Turbulent
②	0.14	0.05	Turbulent	Turbulent
③	0.14	0.01	Turbulent	Laminar
④	0.014	0.09	Laminar	Turbulent
⑤	0.014	0.05	Laminar	Turbulent
⑥	0.014	0.01	Laminar	Laminar

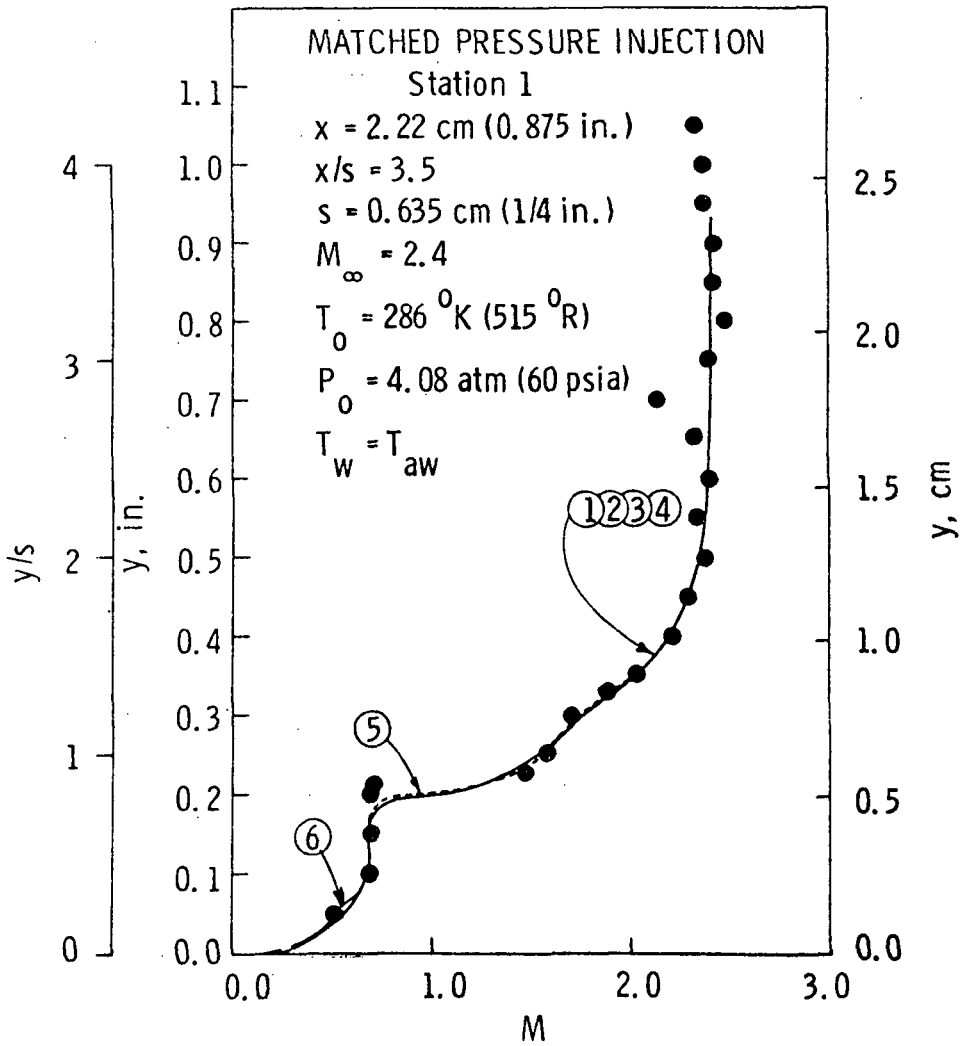

Figure 22: Comparison of Mach Number Profiles with Laminar and Turbulent Slot Flow and Mixing; Station 1, VPI Conditions

- VPI Experiment of Kenworthy and Schetz

Results of Present Method with Beckwith and Bushnell ε^+

Curve	a_j	a_m	SLOT	MIXING
①	0.14	0.09	Turbulent	Turbulent
②	0.14	0.05	Turbulent	Turbulent
③	0.14	0.01	Turbulent	Laminar
④	0.014	0.09	Laminar	Turbulent
⑤	0.014	0.05	Laminar	Turbulent
⑥	0.014	0.01	Laminar	Laminar

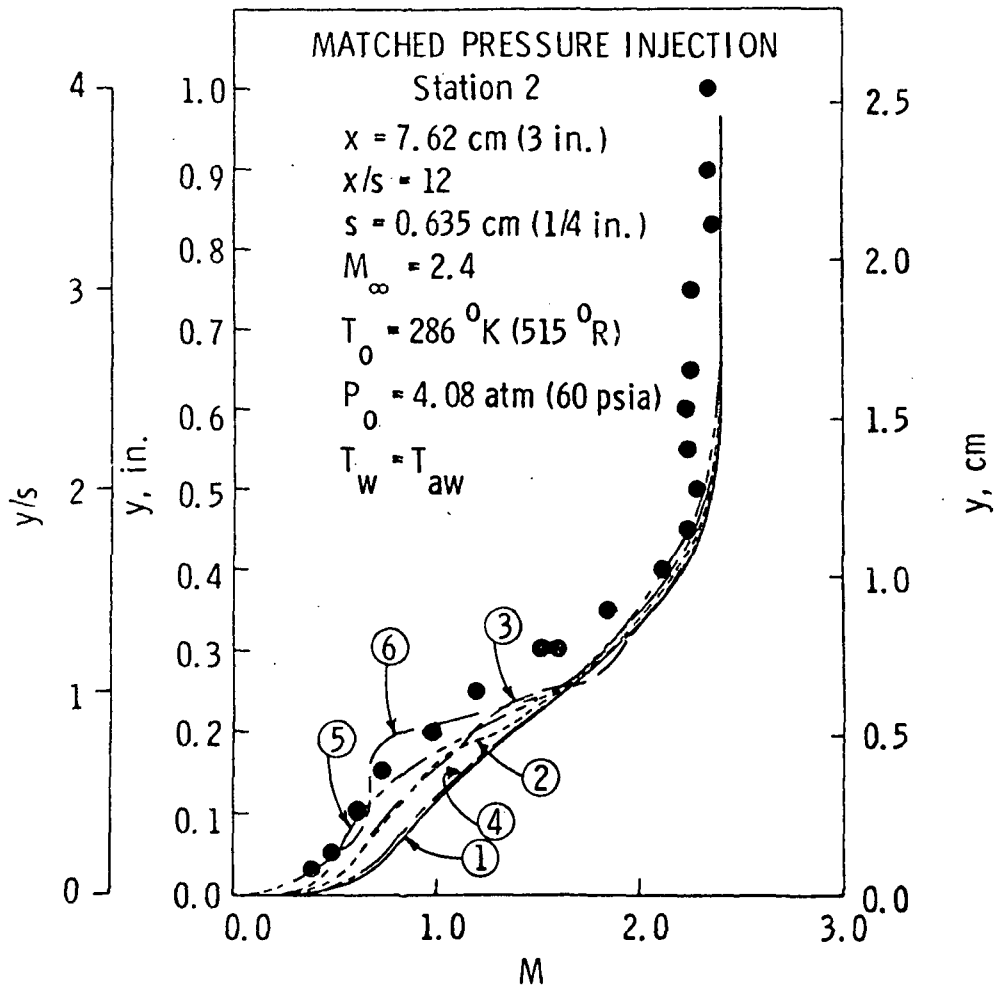

Figure 23: Comparison of Mach Number Profiles with Laminar and Turbulent Slot Flow and Mixing; Station 2, VPI Conditions

- VPI Experiment of Kenworthy and Schetz

Results of Present Method with Beckwith and Bushnell ε^+

Curve	a_j	a_m	SLOT	MIXING
①	0.14	0.09	Turbulent	Turbulent
②	0.14	0.05	Turbulent	Turbulent
③	0.14	0.01	Turbulent	Laminar
④	0.014	0.09	Laminar	Turbulent
⑤	0.014	0.05	Laminar	Turbulent
⑥	0.014	0.01	Laminar	Laminar

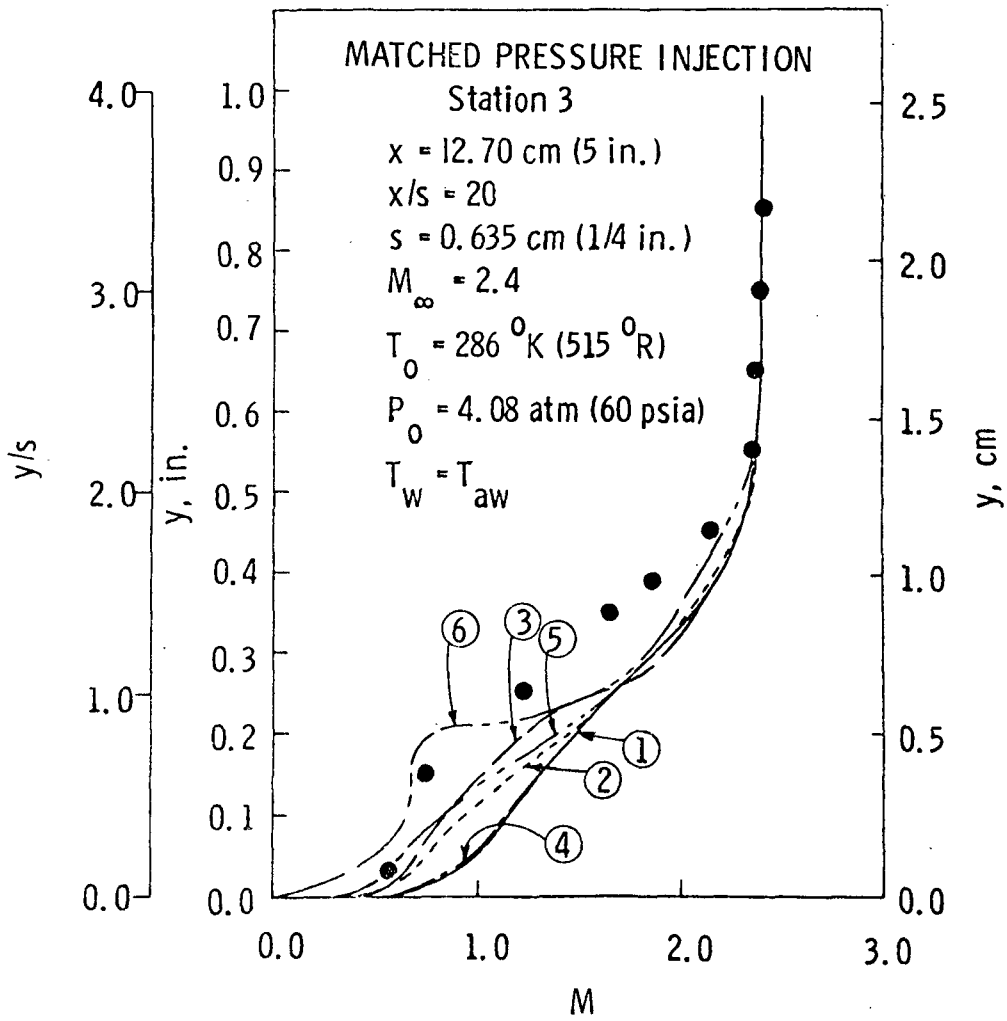

Figure 24: Comparison of Mach Number Profiles with Laminar and Turbulent Slot Flow and Mixing; Station 3, VPI Conditions

- VPI Experiment of Kenworthy and Schetz

Results of Present Method with Beckwith and Bushnell ε^+

Curve	a_j	a_m	SLOT	MIXING
1	0.14	0.09	Turbulent	Turbulent
2	0.14	0.05	Turbulent	Turbulent
3	0.14	0.01	Turbulent	Laminar
4	0.014	0.09	Laminar	Turbulent
5	0.014	0.05	Laminar	Turbulent
6	0.014	0.01	Laminar	Laminar

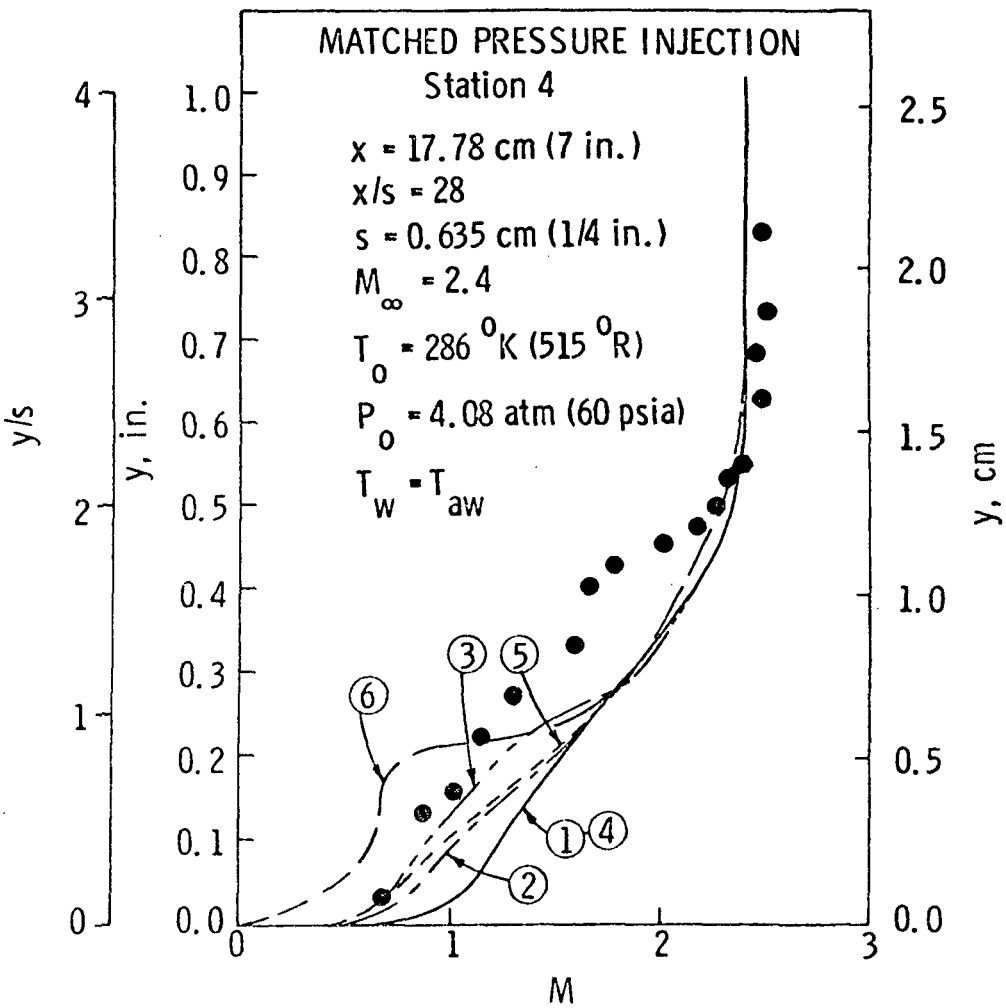

Figure 25: Comparison of Mach Number Profiles with Laminar and Turbulent Slot Flow and Mixing; Station 4, VPI Conditions

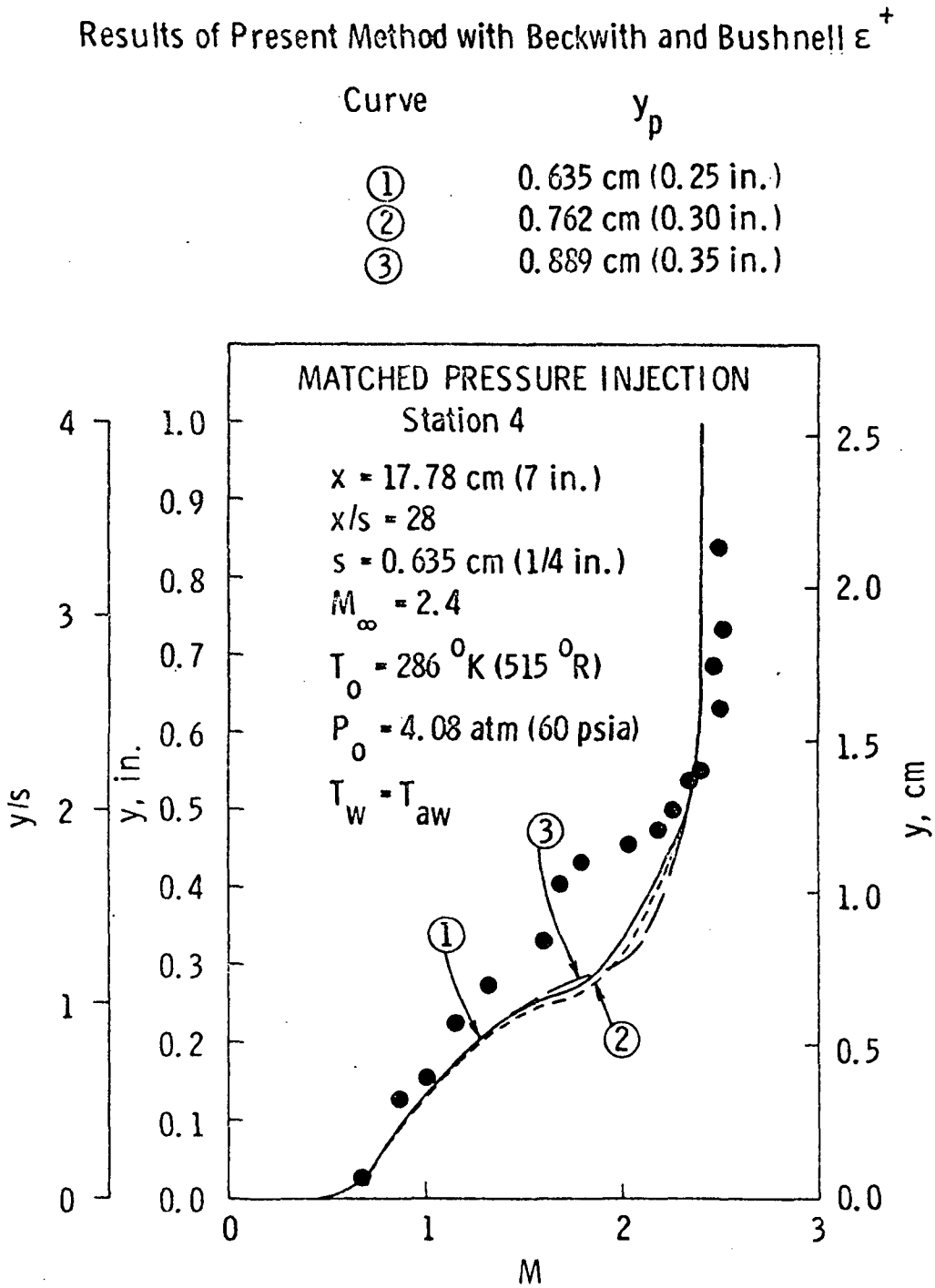

Figure 26: Comparison of Mach Number Profiles with Different Initial Species Concentration Profiles at Station 4 for VPI Conditions

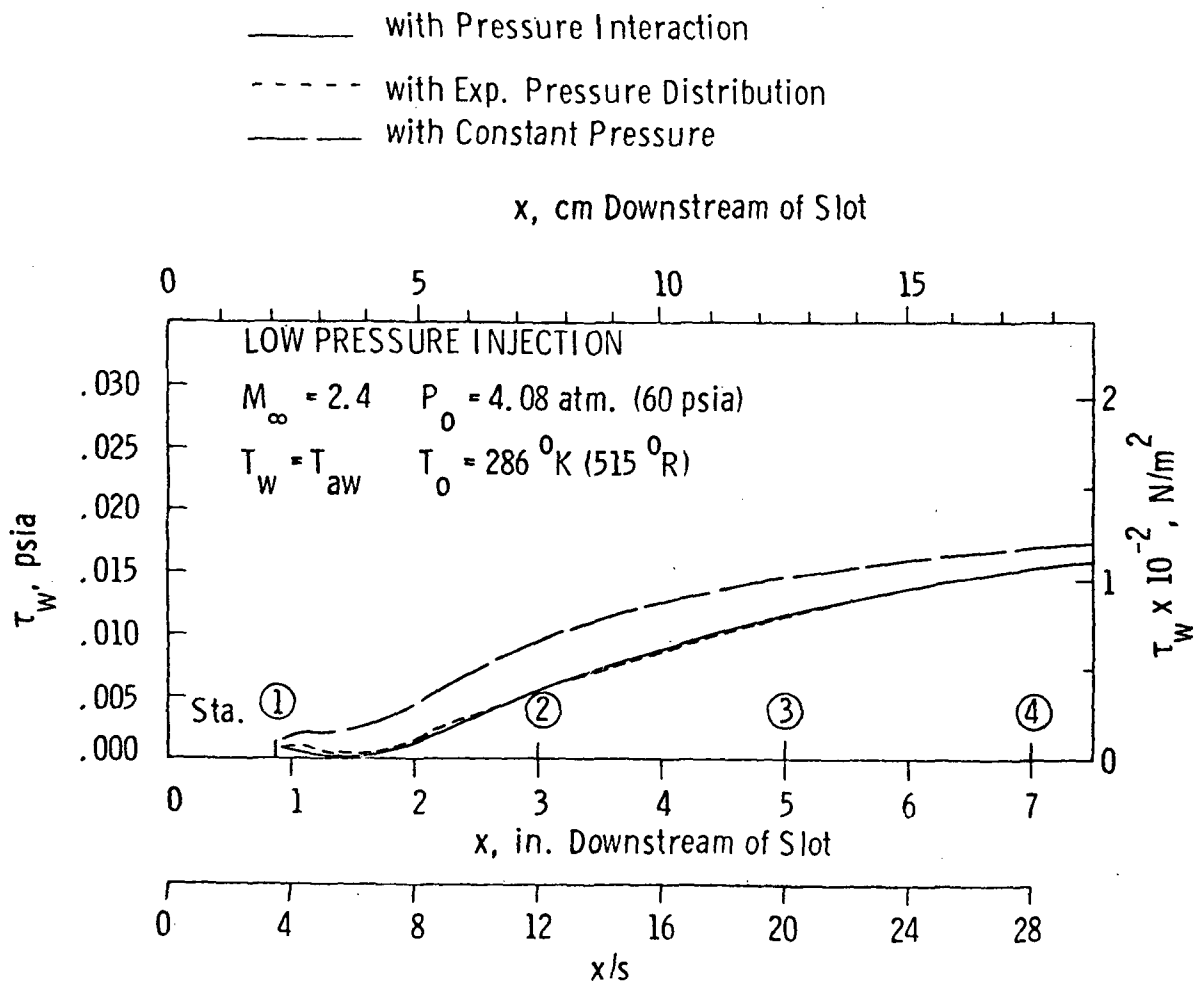

Figure 27: Comparison of Predicted Wall Shear Stress Distributions with and without Pressure Interaction, VPI Conditions, with Beckwith-Bushnell ϵ^+

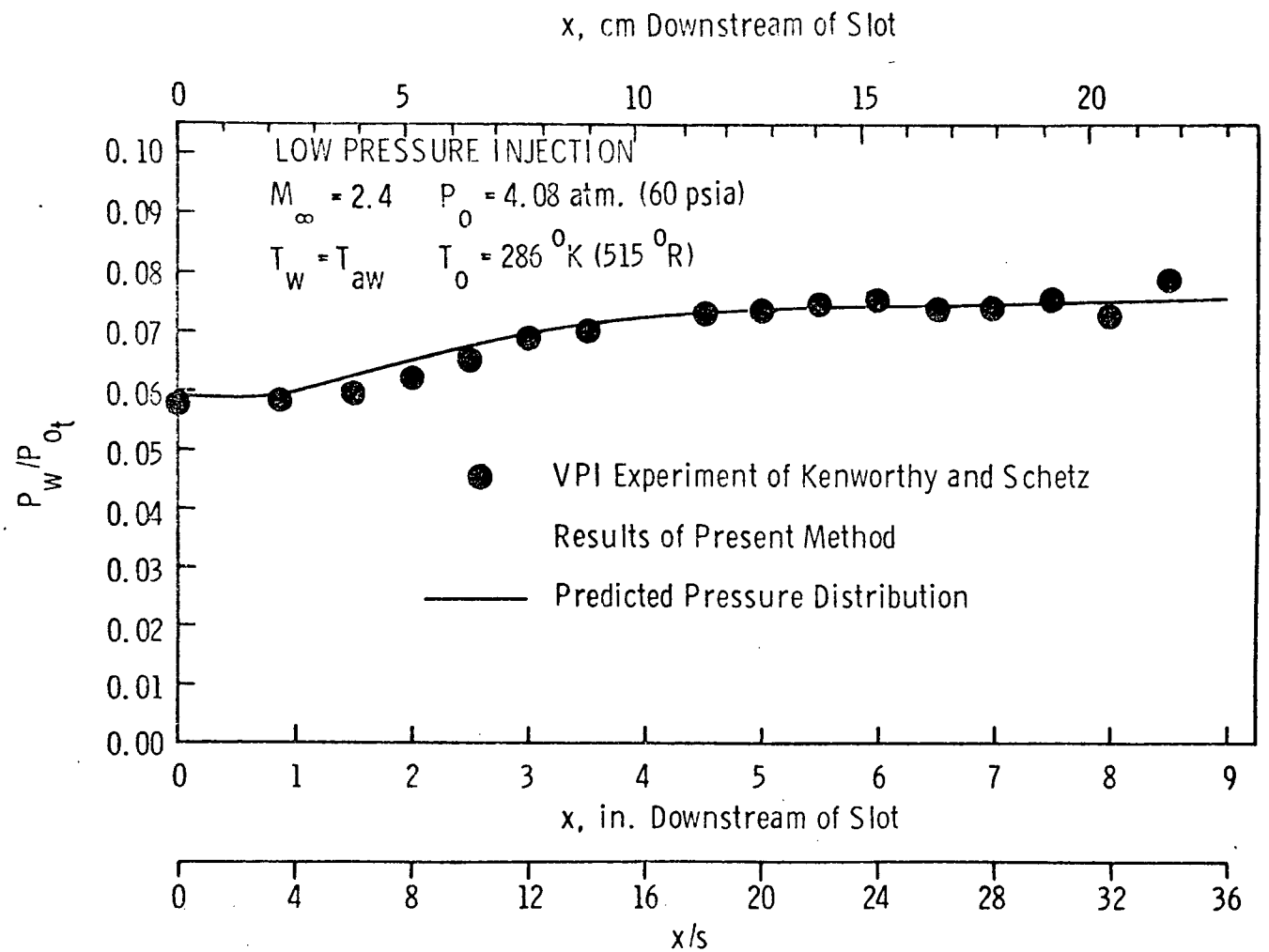

Figure 28: Comparison of Experimental and Predicted Wall Static Pressure Distributions, VPI Conditions

NASA-Langley, 1972 — 12 CR-2124